Forecasting Development

Forecasting Research Technical Report No. 370

Short range contrail prediction

By T.R. Scott, F.I. Hilton, S.L. James and R.W. Lunnon

November 2001

© Crown Copyright 2001

Met Office , Forecasting Development , Room R321, London Road , Bracknell , Berkshire ,RG12 2SZ, United Kingdom

00/0486

Forecasting Research
Technical Report No. 370

Short range contrail prediction

Part A

Verification of short range contrail forecasts

by

T.R. Scott, F.I. Hilton, S.L. James and R.W. Lunnon

Part B

Investigation into the use of Meteosat water vapour channel data in contrail forecasting

by

F.I. Hilton

November 2001

The Met Office
Forecasting Development
Room R321
London Road
Bracknell
RG12 2SZ
United Kingdom

© Crown Copyright 2001

Permission to quote from this paper should be obtained from the above Met Office division

Please notify us if you change your address or no longer wish to receive these publications.

Tel: 44 (0)1344 856245 Fax: 44 (0)1344 854026 email: jsarmstrong@meto.gov.uk

Short range contrail prediction

T R Scott, F I Hilton, S L James and R W Lunnon

November 2001

Part A

Verification of short range contrail forecasts

T R Scott, F I Hilton, S L James and R W Lunnon

Part B

Investigation into the use of Meteosat water vapour channel data in contrail forecasting

F I Hilton

Verification of short range contrail forecasts

T R Scott, F I Hilton, S L James and R W Lunnon

November 2001

Abstract

Short range contrail forecasts calculated from Met Office numerical weather prediction data have been verified against actual contrail occurrence for the eastern region of the North Atlantic flight routes. The contrail occurrence was determined by automated analysis of AVHRR images from the NOAA-14 polar orbiting satellite, and the presence of aircraft to produce the contrails was confirmed using aircraft flight data from NATS. Verification of the forecasts at altitudes where conditions were borderline for contrail formation proved difficult because of aircraft stacking over a range of flight levels. Verification of the forecasts where conditions were non-borderline showed that the non-borderline forecasts may over-forecast but do not under-forecast contrail formation. Thus these non-borderline forecasts could be used to identify regions where contrail formation will not occur, as required for both military and civil aviation purposes.

1 Introduction

Forecasts of contrail formation are of potential interest to both the military and commercial aviation communities. Contrail formation by military aircraft can be undesirable because contrails are easily visible from the ground and can expose clandestine air operations (Peters, 1993). For commercial aircraft it is the environment that is of concern. Contrails can spread and persist for several hours, perhaps triggering widespread cirrus formation. This affects the radiation balance of the atmosphere, and if air traffic increases as projected into the 21st century then contrails could begin to make a significant contribution to climate change (Gierens et al., 1999).

Contrail formation theory is well advanced, having been under development since World War II when contrail existence first became of practical interest. Mathematical models of the contrail formation process (Coleman, 1996; Schumann, 1996; Schrader, 1997) can now be used to predict contrail formation with reasonable accuracy, assuming the availability of accurate data on the meteorological conditions and the aircraft engine characteristics (Jensen et al., 1998).

The requirement for accurate data means that forecasting contrail formation from theory is difficult, particularly if conditions are borderline for contrail formation. Attempts to retrospectively nowcast in-situ observations of contrail occurrence from radiosonde data, numerical weather prediction data, assumed data, or some combination of these, have not been particularly successful (Peters, 1993; Moss, 1999; Walters and Shull, 1999; Jackson et al., 2001). Radiosonde data are unreliable and not always coincident with the contrail observations in either space or time, whereas numerical weather prediction data can be of even lower resolution and also inaccurate.

An alternative forecasting method is to use an empirical relationship between the meteorological conditions and contrail formation. One such relationship has been shown to out-perform the theoretical approach for input data taken from radiosonde ascents (Jackson et al., 2001). However

this relationship was derived and tested using data valid for only a limited range of atmospheric conditions, and empirical techniques might not perform so well under more general use.

This report, funded by the MOD Meteorological Support Unit, investigates whether the Met Office could provide accurate contrail forecasts for military purposes. These forecasts would be calculated from theory using Met Office numerical weather prediction data. Trial forecasts are verified against contrails observed over a wide area in satellite images. The area selected for study was the region of the North Atlantic between 50°W to 0°W and 45°N to 60°N, which contains the eastern section of the North Atlantic flight routes.

Section 2 of this report describes the various data sets used for the project, and discusses the problems associated with them. These data sets were converted into a common data format for comparison purposes, and this process is described in section 3. Section 4 contains the verification of the forecasts, where the ability of the forecasts to predict contrail formation is assessed. The conclusions of the report are presented in section 5. A glossary of acronyms is given in appendix A.

2 The data

Three types of data were used to verify contrail forecasts calculated from Met Office NWP data. These data were:

1. The *expected* occurrence of contrails. This is defined as the contrail occurrence that would be expected to be observed under the assumption that all aircraft produce contrails, even if the meteorological conditions are unsuitable for contrail formation.

2. The *detected* occurrence of contrails. This is defined as the actual observed contrail occurrence.

3. The contrail *forecasts*. These are the predictions as to whether the meteorological conditions are suitable for contrail formation.

The contrail *forecasts* should account for any differences between the *expected* and *detected* contrail occurrence, as the expected contrails should not be detected unless the meteorological conditions are suitable for contrail formation.

The remainder of this section discusses the generation of these data, the scope of their validity, and the problems associated with them. It begins with the detected contrails, moves onto the expected contrails, and ends with the contrail forecasts. This order is used because the times for which contrail observations were available determined the times for which the expected contrails and contrail forecasts were required.

2.1 Detected contrails

Satellite observations were used to detect the actual occurrence of contrails. They were used in preference to the in-situ observations used in previous studies primarily because of their ready availability. However their wide spatial coverage and frequent temporal updates also meant that contrail occurrence could be observed for a larger range of meteorological conditions than would have been possible using more limited in-situ observations.

Contrails appear in infrared images as cold clouds with a distinctive linear shape. Images used for contrail detection are frequently those from the AVHRR instruments on board the NOAA-series of

polar orbiting satellites. These images have a high resolution of 1.1 km at the sub-satellite point so that contrails can be resolved. They are also available in split infrared channels, which is useful for contrail detection because the contrast of the contrails against their background is enhanced in the brightness temperature difference between the two channels (Lee, 1989; Betancor Gothe and Graßl, 1993).

The existence of contrails in satellite images can be determined by visual inspection (Bakan et al., 1994) or by use of a contrail detection algorithm (Engelstad et al., 1992; Mannstein et al., 1999). The latter approach is preferable because it is consistent and avoids manual examination of each image of interest. However developing and implementing a detection algorithm requires significant effort. Fortunately the benefit of using a detection algorithm was gained without developmental cost because the contrail detection algorithm of Mannstein et al. (1999) was kindly made available for use on the project (Meyer, 2000a).

The Mannstein et al. algorithm uses images from the split infrared AVHRR channels for contrail detection. These channels are channel 4 ($10.3 - 11.3\,\mu$m) and channel 5 ($11.5 - 12.5\,\mu$m). The images must be in original projection as seen from the satellite, as contrails may become unresolvable in reprojected data.

2.1.1 The AVHRR images

Data from NOAA-series satellites are sent to the Met Office from Lasham satellite tracking station in Hampshire. Data for a particular satellite pass arrive shortly after completion of that pass and are in what is known as HRPT format. This format contains raw data from all of the satellite instruments and requires further processing before use.

Images suitable for use by the detection algorithm were obtained by processing the HRPT data using the AAPP software package distributed by EUMETSAT. This package can be used to produce calibrated AVHRR images in their original projection, together with navigation information from which the latitudes and longitudes corresponding to each image pixel can be calculated.

Satellite passes selected for use were those having reasonable coverage of the eastern North Atlantic on days between September and December 2000 inclusive for which air traffic data were available. These days were the 4th and 15th of each month.

A total of 29 passes were acquired and processed for contrails. These passes are listed in table 1. A channel 4 image for the 1648 GMT satellite pass on 04 October 2000 is shown in figure 1.

2.1.2 The contrail detection algorithm

The contrail detection algorithm of Mannstein et al. (1999) searches for contrail-like features in the brightness temperature difference between AVHRR channels 4 and 5. The output is a binary image showing the pixels in the satellite image that contain detected contrails. The algorithm was successfully implemented at the Met Office following conversion of the software from IDL to PV-Wave. It was run with identical parameters to those described in Mannstein et al.

The results of applying the algorithm to a small section of data from the 1648 GMT pass on 04 October 2000 are shown in figure 2.

Date (in 2000)		Pass number	Time (GMT)
04	September	29276	0603
04	September	29277	0744
04	September	29282	1556
04	September	29283	1739
15	September	29431	0535
15	September	29432	0716
15	September	29437	1528
15	September	29438	1710
04	October	29699	0513
04	October	29700	0654
04	October	29706	1648
15	October	29854	0445
15	October	29855	0626
15	October	29856	0807
15	October	29861	1619
15	October	29862	1803
04	November	30137	0552
04	November	30138	0733
04	November	30143	1545
04	November	30144	1727
15	November	30292	0523
15	November	30293	0704
15	November	30299	1657
04	December	30561	0641
04	December	30562	0822
04	December	30567	1634
15	December	30716	0611
15	December	30717	0752
15	December	30722	1604

Table 1: NOAA-14 satellite passes used for contrail detection. The time is the acquisition time for the first row of data. The number of acquired rows depends on the time for which the satellite remains visible to the tracking station, which is roughly 15 minutes. Data acquisition is either from north to south or from south to north.

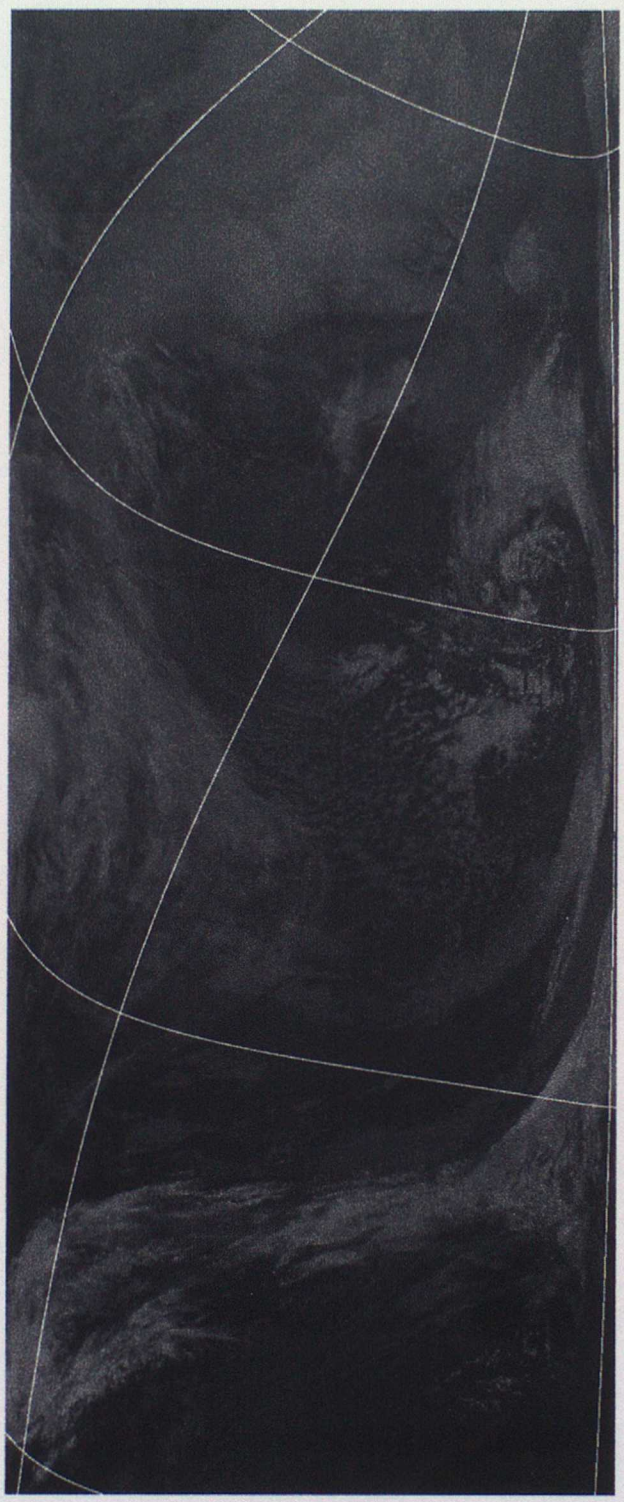

Figure 1: Channel 4 image in original projection for a NOAA-14 satellite pass from south to north beginning at 1648 GMT on 04 October 2000. Lighter colours correspond to colder brightness temperatures. The image is of size 2000 by 4880 pixels. The resolution at the sub-satellite point, corresponding to the central column in the image, is 1.1 km. The resolution decreases for columns nearer the edge. The longitude contours from left to right are 50°W, 25°W and 0°W and the latitude contours from bottom to top are 30°N, 45°N, 60°N and 75°N.

Channel 4 brightness temperature

Channel 5 brightness temperature

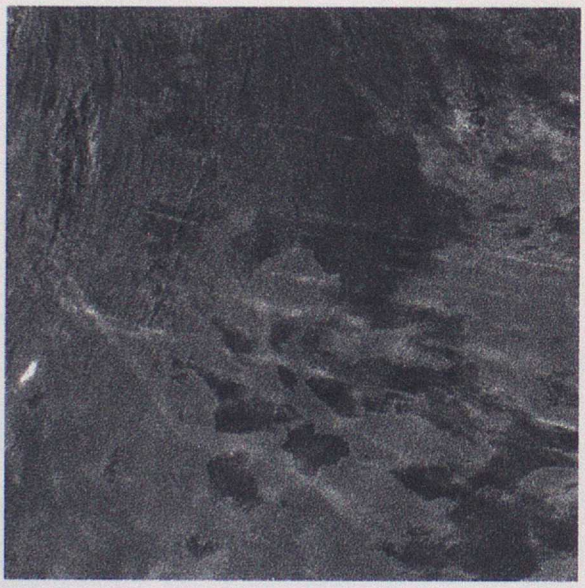

Brightness temperature difference between channels 4 and 5

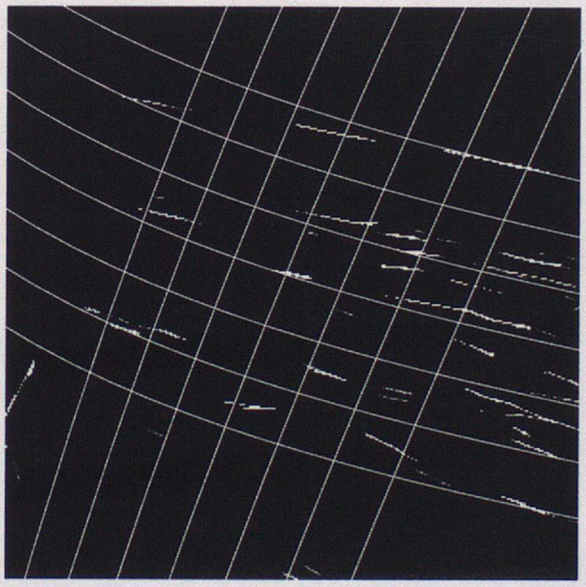

Detected contrails

Figure 2: Contrails detected in a small section of data from the 1648 GMT satellite pass on 04 October 2000. Although the contrails are partly obscured by cirrus cloud in both channels 4 and 5, they stand out in the brightness temperature difference and are successfully identified by the contrail detection algorithm. The latitude and longitude lines plotted over the detected contrails outline grid cells in the Met Office's global NWP model. Their relevance is discussed in section 3.

2.1.3 Detection efficiency

Not all contrails are detectable in AVHRR images. Some will be obscured by cloud, some will not be resolved, and others will not be correctly identified by the contrail detection algorithm.

When contrails initially form they are trapped within wake-vortices at the wing-tips of the aircraft, where they remain narrow and hence unresolvable in AVHRR images (Gerz et al., 1998). As the wake-vortices dissipate the contrails become mixed with the ambient air and usually sublimate. Only if the ambient air is supersaturated with respect to ice will the contrails persist and spread, becoming detectable in AVHRR images about 10 minutes after formation. As the persistent contrails age they begin to lose their linear shape and become optically thinner, thus becoming less identifiable by the contrail detection algorithm. Contrails older than about 100 minutes are increasingly unlikely to be detected (Meyer, 2000b).

The false alarm rate for the algorithm is estimated to be 0.1% of the coverage for observations made over the sea, such that for every 1000 image pixels 1 pixel will be wrongly classified as containing a contrail (Mannstein et al., 1999). The false alarm rate increases significantly towards the edges of the images where the viewing angle is high. For this reason contrail detections within 100 columns of either side of an image are unreliable. The false alarms are usually elongated cirrus streaks (Meyer, 2000b) and are likely to be correlated with contrail forming regions because contrails are similar to cirrus and tend to form under similar meteorological conditions.

2.1.4 Detection coverage

The contrail detection coverage is the region of the AVHRR pass where contrails can be reliably detected. It excludes a border around the image of width 29 pixels where contrails cannot be detected because of edge effects, and regions within 19 pixels of an image row that has been identified by the algorithm as containing corrupt data, because these data will have affected the detection process. It also excludes 100 columns on either side of the image because of the high false alarm rate in these regions, as mentioned above.

2.2 Expected contrails

The expected locations of contrails at any given time can be calculated from aircraft flight paths and wind velocity data. Wind will advect contrails away from their initial place of formation, by an amount that depends on the wind velocity and the elapsed time since formation.

2.2.1 Aircraft flight data

Aircraft movements in Shanwick airspace, which covers the eastern region of the North Atlantic flight routes, are archived by NATS on the 4th and 15th of each month. Data were acquired for the months of September to December 2000 inclusive. They consisted of aircraft latitude-longitude-altitude-time location coordinates, with a maximum of 8 locations per aircraft.

2.2.2 Aircraft flight data coverage

The data provided by NATS were bounded to the north, south and east by the edges of Shanwick airspace. However the data appeared to extend further west than the Shanwick border. Examina-

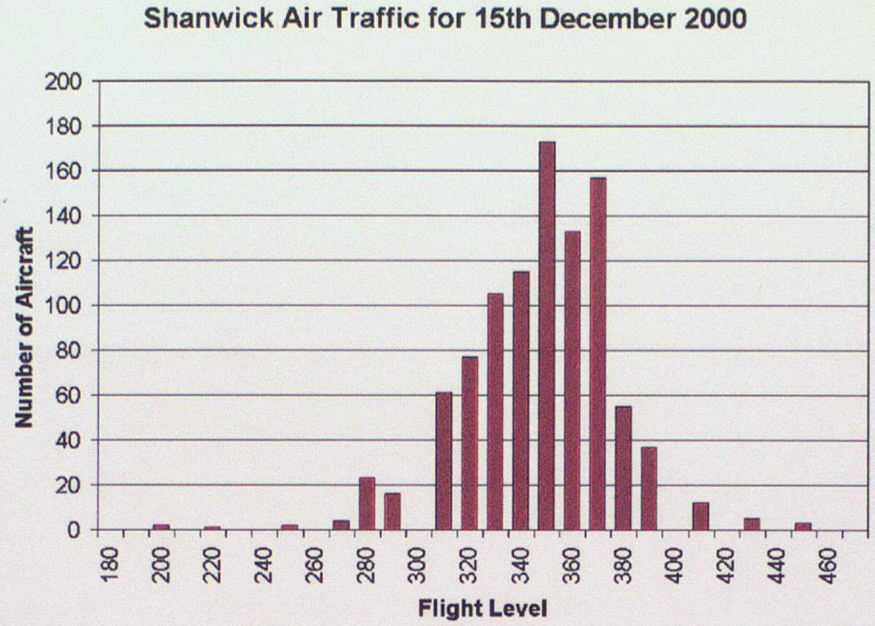

Figure 3: Typical distribution of aircraft flight levels over the North Atlantic, generated from Shanwick airspace flight data provided by NATS for 15 December 2000.

tion of the data showed that it was reliably available out to 40°W. The aircraft coverage was thus taken to be Shanwick airspace extended to 40°W.

Aircraft fly on designated flight levels denoted by FLxxx. These flight levels are actually pressure levels, where xxx is the altitude in units of 100 ft that an aircraft would have if it were flying in a ICAO standard atmosphere. Over the North Atlantic the flight levels are separated by nominal vertical distances of 100 ft. The flight levels most in use lie between FL310 and FL390 inclusive, which roughly correspond to pressure levels of 300 and 200 hPa respectively. The flight level distribution can be seen in figure 3, which was generated from the NATS data.

2.2.3 Aircraft time windows

A contrail will only be detectable in an AVHRR image if it was formed between about 10 and 100 minutes prior to the acquisition time of the image, as discussed in section 2.1.3. Thus only aircraft flying within this time window are of interest. However, the time window used for processing the data was actually between 10 and 90 minutes. This shortening of the time window was unintentional but unlikely to greatly affect the verification results.

For each satellite pass given in table 1, aircraft flying in the required time window were identified and their spatial coordinates at each end of the window calculated. This was usually done by interpolating between the NATS locations, but when this was not possible the nearest NATS location was taken. No extrapolation was performed because aircraft can change flight orientation or speed between reporting points. For each aircraft the two end point locations, together with any NATS locations that lay between them, then defined the flight track traversed by the aircraft during the time window.

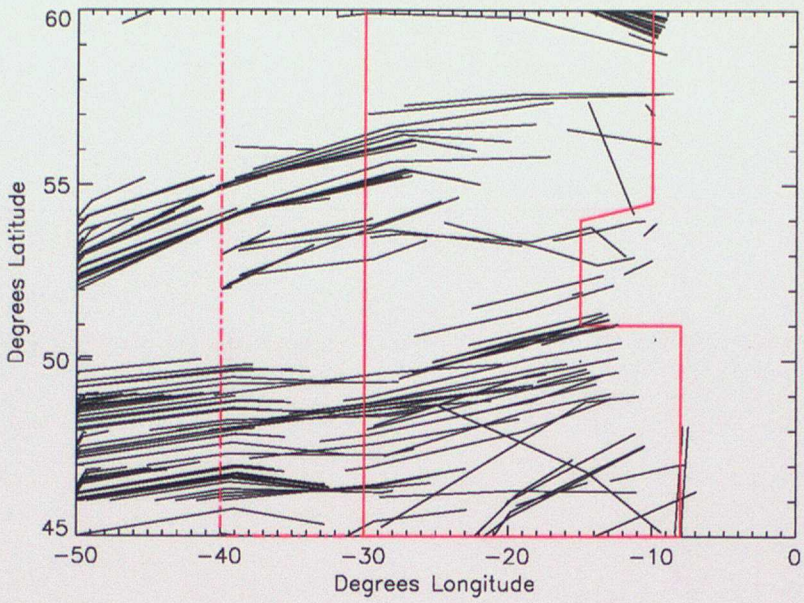

Figure 4: Expected contrails for the 1648 satellite pass on 04 October 2000. These are the contrails that are expected to be present in the AVHRR image assuming that all aircraft actually produce contrails. The solid red line outlines Shanwick airspace for which NATS flight data were supplied. The dashed red line outlines a westwards extension to Shanwick which was also reliably covered by the NATS data.

2.2.4 Flight path advection

In windless conditions a contrail produced by an aircraft will lie along the aircraft flight track. However when there is wind the contrail will be advected away from this track, by an amount equal to the wind velocity multiplied by the elapsed time since contrail formation. Thus the older end of a contrail will always be displaced further from the aircraft track than the newer end, assuming that the wind velocity is constant in both space and time.

The locations defining the aircraft flight tracks were advected using NWP wind fields (described in section 2.3) valid at the time of the AVHRR image. The advected locations then defined the contrails expected to be observed in the AHVRR image, under the assumption that all of the aircraft produced contrails regardless of the meteorological conditions.

The expected contrails for the 1648 GMT satellite pass on 04 October 2000 are shown in figure 4, for flight levels FL310 to FL390 inclusive. Overplotted on the figure is an outline of Shanwick airspace and its westwards extension.

2.2.5 Accuracy of expected contrails

The positional accuracy of the expected contrails is limited by both the aircraft flight data and the NWP wind data. The latitude of an aircraft is only reported to within ±0.5°, and the NWP wind data may not accurately represent the actual wind conditions. These error sources could result in positional errors much greater than the resolution of the AVHRR images.

It was hoped that it would be possible to match the expected contrails with the detected contrails so that the altitude of the detected contrails could be determined. This would have aided verification

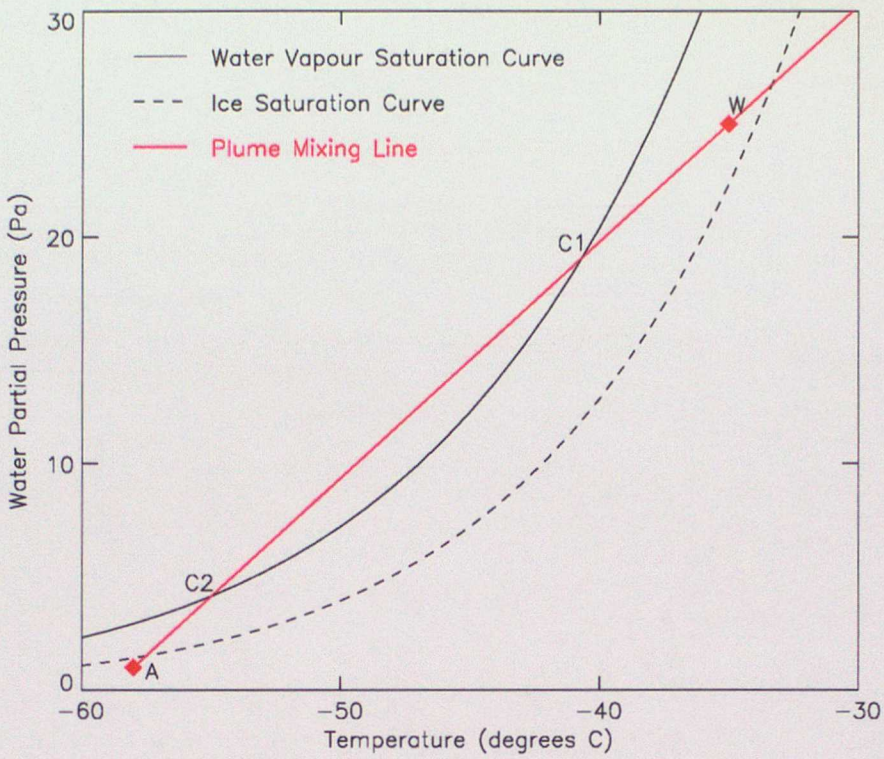

Figure 5: The red line in this figure represents the cooling and drying of an aircraft exhaust plume as it mixes with the ambient air. The initial conditions in the plume are outside the top-right of the figure, and the ambient air conditions are represented by point A. The slope of the line is equal to the contrail factor. The solid and dashed lines are respectively the saturation vapour pressures over water and ice. A contrail will form between C1 and C2 where the conditions in the plume are saturated with respect to water. At point W the plume is supersaturated with respect to ice but a contrail will not form because saturation with respect to water is required (Kärcher et al., 1998; Jensen et al., 1998).

of the contrail forecasts as the variation of the forecasts with altitude could have been accounted for. However contrail matching proved difficult because of the positional errors in the expected contrails, and also because of air traffic density. There were usually several aircraft stacked at different altitudes along the same flight path which made assignment of a detected contrail to a unique flight level extremely difficult.

In a few cases it was possible to match expected contrails with detected contrails by visual inspection. This demonstrated accurate spatial and temporal alignment of the expected and detected contrail data.

2.3 Contrail forecasts

Contrails form when water vapour in the exhaust of the aircraft condenses and freezes on mixing with the ambient air (Schumann, 1996). The ability to forecast contrails thus depends on accurately knowing the atmospheric conditions in both the aircraft exhaust and the ambient air, and on having an equation to accurately represent the mixing process. This mixing process is illustrated in figure 5.

Contrail formation is usually forecast in terms of a critical temperature T_c such that contrails will form if the ambient air temperature T is colder than this critical value i.e., $(T - T_c) < 0$.

The equation used to calculate the critical temperature for this project was derived by Moss (1999). It has as independent variables the pressure and humidity mixing ratio of the ambient air, and a variable relating the conditions in the aircraft exhaust to the conditions in the ambient air. This variable is called the contrail factor and is defined as the ratio of the increase in humidity mixing ratio to the increase in temperature above ambient in the exhaust of the aircraft. The contrail factor depends on engine type and it was assumed to be that given by Moss for a high-bypass engine, since this is the engine type used by civilian jet aircraft.

Data for input to the critical temperature equation were obtained from NWP modelling. Pressures were taken directly from the model, but the humidity mixing ratios had to be calculated from model relative humidities and temperatures, thus effectively bringing temperature dependence into the critical temperature equation. These data were used to calculate forecasts of contrail formation for times corresponding to the satellite pass times given in table 1. The forecasts covered the area 50°W to 0°W and 45°N to 60°N, and were for several altitudes and several forecast lead times. The following sections describe exactly which forecasts were calculated from which NWP data, with examples again being given for the 1648 GMT satellite pass on 04 October 2000.

2.3.1 NWP modelling

A NWP model is a mathematical model of the atmosphere with an initial state that represents the atmospheric conditions at a particular time. From this initial state the model can be used to forecast the atmospheric conditions at some future time.

The initial state is known as the analysis and is calculated by adjusting a previous forecast so that the adjusted forecast better matches recent observations. Analyses are calculated somewhat after their validity time to allow time for the observational data to be received.

Forecasts made from an analysis to a future time are typically referred to in the form xxZ + Tyy, where xx is the time of the analysis and yy is the lead time of the forecast, i.e., the number of hours ahead that the forecast is valid. A 12Z+T06 forecast will thus have been calculated from a 1200 GMT analysis, will have a lead time of 06 hours, and will be valid at 1800 GMT. For convenience an analysis can be considered as being a forecast with a lead time of 00 hours and denoted as such.

NWP data covering the North Atlantic are available from the Met Office's global model. These data are defined on a latitude-longitude-pressure grid, with a latitude resolution of $0.55\dot{5}$ degrees and a longitude resolution of $0.83\dot{3}$ degrees. Model pressure levels that correspond to the aircraft flight levels of interest are 300, 250 and 200 hPa.

For this project two types of global model forecasts were of interest: Global Update forecasts and Preliminary Global forecasts.

Global Update forecasts

Global Update analyses are calculated 4 times per day for analysis times of 00Z, 06Z, 12Z and 18Z, and used to forecast up to 6 hours ahead in time steps of 3 hours. The Global Update analyses incorporate more observation data than do any other global model analyses and therefore best represent the state of the atmosphere at the analysis time. However the forecasts only become available about 8 hours after the analysis time, making them unsuitable for operational forecasting. They are best used retrospectively to represent the actual atmospheric conditions at a given place and time.

Preliminary Global forecasts

Preliminary Global analyses are also calculated 4 times per day for the same analysis times as the Global Update analyses. Forecasts are made up to 48 hours ahead in times steps of 3 hours. The analyses are calculated shortly after the analysis time and the forecasts become available just 3 hours after this time. This makes them suitable for short-range operational forecasting.

2.3.2 Retrospective forecasts

To assess the performance of the critical temperature equation independently of lead time associated errors in the input data, contrail forecasts were first calculated using the best available data from Global Update forecasts.

For a given satellite pass there always exist two recent Global Update forecasts with validity times 3 hours apart bracketing the time of the satellite pass. These are either T+00 and T+03 forecasts, or T+03 and T+06 forecasts. Interpolation between these two forecasts gives the atmospheric conditions at the actual time of the satellite pass. Interpolation between the model pressure levels then gives the atmospheric conditions at the aircraft flight levels.

Temperature and relative humidity data from these interpolated Global Update forecasts were used to calculate contrail formation forecasts of $(T - T_c)$ using the critical temperature equation. These retrospective forecasts will be termed the F00 contrail forecasts. Wind data were also used to perform the advection of the aircraft flight tracks as described in section 2.2.4.

As an example, for the 1648 GMT satellite pass on 04 October 2000 input data for the critical temperature equation were found by interpolating between the Global Update 12Z+T03 and 12Z+T06 forecasts and then interpolating from pressure to flight levels.

2.3.3 Operational forecasts

Contrail forecasts that could have been made available on an operational basis were also calculated for each of the satellite passes. The input data used for these forecasts were taken from Preliminary Global forecasts valid within 3 hours of the satellite pass, for lead times of 06, 12 and 24 hours. The data were not interpolated to the time of the satellite pass, but were once again interpolated vertically to the aircraft flight levels.

These operational contrail forecasts will be termed the F06, F12 and F24 contrail forecasts.

Continuing the example for the 1648 GMT satellite pass, F06, F12 and F24 contrail forecasts were calculated from 12Z+T06, 06Z+T12 and 18Z+T24 Preliminary Global model data, for 12Z and 06Z analyses on 04 October 2000 and an 18Z analysis on 03 October 2000.

2.3.4 Problems with forecast calculation

Contrail forecast accuracy depends on the ability of the critical temperature equation to model the contrail formation process, and on the way in which this equation is implemented. Several problems with the implementation used in this project were identified.

Conversion of relative humidities to humidity mixing ratios

NWP relative humidities were converted to humidity mixing ratios assuming relative humidities with respect to water. However for temperatures colder than freezing the Met Office NWP relative humidities are with respect to ice. Saturation over ice occurs before saturation over water, as can be seen in figure 5, so the calculated humidity mixing ratios will have been too high. This means that the forecasts will have over-estimated the size of contrail formation regions.

Contrail factor differences between aircraft

The contrail factor, which specifies the gradient of the mixing line shown in figure 5, is essentially a measure of engine propulsion efficiency. Propulsion efficiency η is the ratio of the energy used to propel an aircraft to the energy supplied by the aircraft fuel (Schumann et al., 2000). The energy lost to heat is proportional to $(1-\eta)$ and this heat increases the temperature of the exhaust plume and hence decreases the contrail factor. Thus more efficient engines form contrails at warmer ambient temperatures. Propulsion efficiency depends on various variables, including the bypass of the engine and the aircraft air speed, and it can vary throughout a flight.

Most contrail prediction methods, including that used here, set the contrail factor according to whether a high-, low-, or non-bypass engine is in use, where high-bypass engines are the most efficient. However propulsion efficiency actually varies on a continuous scale, and it will not be the same of all transatlantic aircraft.

The use of an incorrect contrail factor will either increase or decrease the critical temperature, and hence the regions where contrails are forecast to occur will be either too large or too small, depending on the aircraft. This problem would not exist for forecasts generated operationally for military customers, since in this situation the engine characteristics of the aircraft would be known.

Relative humidity and temperature errors

The temperature and relative humidity data used to calculate the contrail forecasts are subject to errors which will impact on forecast accuracy.

To assess this impact $(T-T_c)$ was calculated on three pressure levels for a range of temperatures and relative humidities. The results are shown in table 2. For each pressure level the central temperature in the table is the ICAO standard temperature for that level, and the surrounding temperatures are the central temperature plus or minus the approximate temperature error standard deviation. This error is for short range global model forecasts as verified against radiosonde measurements (Forrester, 2001). The approximate absolute standard deviation for the relative humidity errors is 25%.

From the table it can be seen that when conditions are borderline for contrail formation $(T-T_c)$ is about equally sensitive to errors in the relative humidity data and errors in the temperature data. Either type of error could alter the forecast outcome.

The table also shows that at altitudes above approximately 250 hPa contrails will usually be expected to form unless the ambient air is particularly warm and dry.

300 hPa (~FL300)		Relative humidity (%) 0	25	50	75	100
T (°C)	-43.0	6.73	4.97	3.20	1.44	-0.33
	-44.5	5.23	3.74	2.24	0.74	-0.76
	-46.0	3.73	2.47	1.20	-0.07	-1.33

250 hPa (~FL340)		Relative humidity (%) 0	25	50	75	100
T (°C)	-50.8	0.64	-0.23	-1.11	-1.98	-2.86
	-52.3	-0.86	-1.59	-2.32	-3.05	-3.79
	-53.8	-2.36	-2.97	-3.58	-4.19	-4.80

200 hPa (~FL390)		Relative humidity (%) 0	25	50	75	100
T (°C)	-55.0	-1.51	-2.17	-2.83	-3.49	-4.15
	-56.5	-3.01	-3.56	-4.11	-4.65	-5.20
	-58.0	-4.51	-4.96	-5.42	-5.87	-6.32

Table 2: $(T - T_c)$ as a function of pressure, temperature and relative humidity, where T is the temperature and T_c is a critical temperature such that contrails will form if $(T - T_c) < 0$. The three central temperatures are the ICAO standard temperatures for the corresponding pressure levels. The adjustments about the central temperature approximately correspond to the error standard deviation for short range global model forecasts at these levels, as verified against radiosonde measurements (Forrester, 2001). The approximate error standard deviation for the relative humidities at these levels is 25%.

2.3.5 Dealing with the relative humidity errors

Before the sensitivity of the critical temperature equation to the NWP data errors had been assessed, it was thought that the relative humidity errors would be the most significant due to their large magnitude. Two methods for dealing with these errors were therefore considered.

Error reduction

The first method was to reduce the magnitude of the errors by adjusting the data according to up-to-date water vapour images from Meteosat or Meteosat Second Generation satellites. However the study presented in Part B of this report found that this would not lead to a significant improvement in forecast accuracy so that implementation of this method would not be worthwhile.

Incorporation of errors into forecasts

The second method was to incorporate the errors into the contrail forecasts. This method was implemented as follows. The F00, F06, F12 and F24 forecasts were recalculated with various adjusted relative humidities. These adjusted relative humidities were the original values with relative percentage reductions and increases of 5%, 10%, 20% and 50%. The resulting 9 forecasts were then combined together into 1 forecast giving the driest adjustment for which contrails were still forecast to occur.

The 9 adjusted F00 forecasts for the 1648 GMT pass on 04 October 2000 are shown in figure 6 for flight level FL310. They are to be compared with the combined forecast for this flight level as shown in figure 7.

Also shown in figure 7 are the combined F00 forecasts for the other flight levels most in use over the North Atlantic. It is interesting that for the higher flight levels the forecasts become independent of the relative humidity adjustment. This independence is typical. At these altitudes the temperature is generally so cold that contrail formation will occur regardless of the relative humidity. The regions for which contrail formation is not forecast are possibly intrusions of warm dry stratospheric air, with relative humidity so low that even if it were 50% higher then contrails would still not form. These intrusions seem to extend down through all of the flight levels of interest. Some of the temperature and humidity data used to calculate the forecasts are shown in figure 8. A possible stratospheric intrusion can be seen in the upper right corner of the data.

In retrospect, the humidity adjustments described above should have been absolute rather than relative, with the adjusted relative humidities having floor and ceiling values of 0 and 100% respectively. Relative adjustments could be small compared to the relative humidity errors that could actually occur, particularly if the atmosphere is dry.

3 Common data format

In order to perform a quantitative verification of the contrail forecasts it was necessary to convert the detected contrails, expected contrails and contrail forecasts into a common data format.

The horizontal resolution of the data was limited by the global model grid of the contrail forecasts, so the detected and expected contrails were mapped onto this grid. At North Atlantic latitudes each model grid cell is of approximate size 60 km × 60 km.

In the vertical the data resolution was limited by the detected contrails, for which no height information was available. The expected contrails and the contrail forecasts were therefore combined together at each flight level and the vertical resolution removed by compressing through the flight levels.

3.1 Detected contrail mapping

A global model cell was classified as a detected contrail region if any contrails were detected within the area represented by that cell. This mapping caused significant loss of detail of the detected contrails since the contrail resolution was effectively reduced from 1.1 km to 60 km.

A global model cell was also classified as a detected contrail coverage region if all of the area represented by that cell had detected contrail coverage. As discussed in section 2.1.4 the detected contrail coverage is the coverage of the AVHRR image where reliable contrail detection can be performed. It changes from satellite pass to satellite pass and so it needs to be specified for each pass of interest.

The mapping result for the 1648 GMT satellite pass on 04 October 2000 is shown in figure 9. This figure is to be compared with figure 2, which shows the actual detected contrails with the global model cells overlaid. The corresponding detected contrail coverage is shown in figure 10. The detected contrail coverage has been used to mask figure 9 to ensure that there are no detected contrails outside the coverage region.

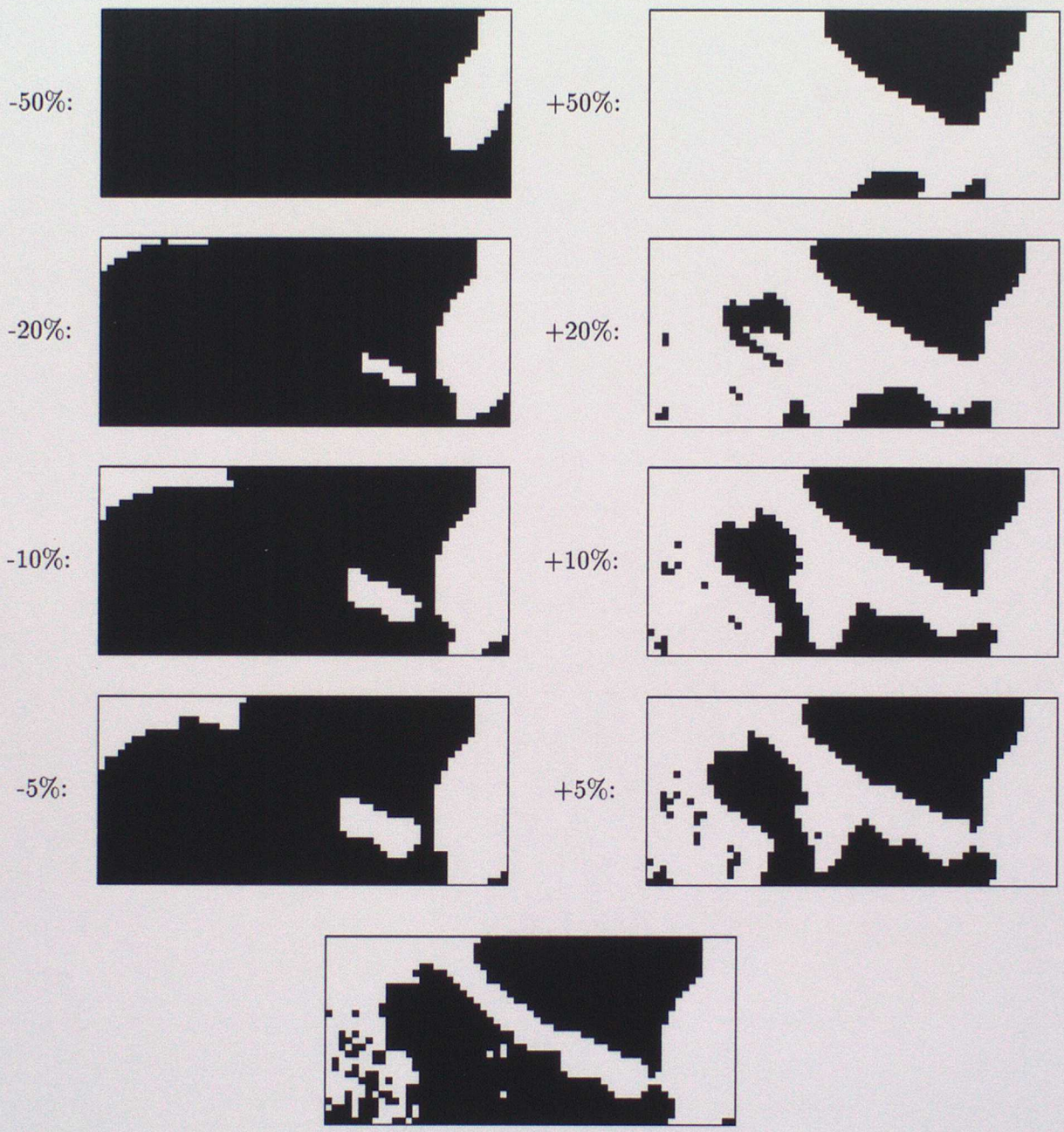

Figure 6: F00 forecasts of contrail formation at flight level FL310 for various relative adjustments of the NWP relative humidity data, from -50% to +50%. The contrail formation regions are shown in white and they grow in size as the humidity is increased, as is to be expected.

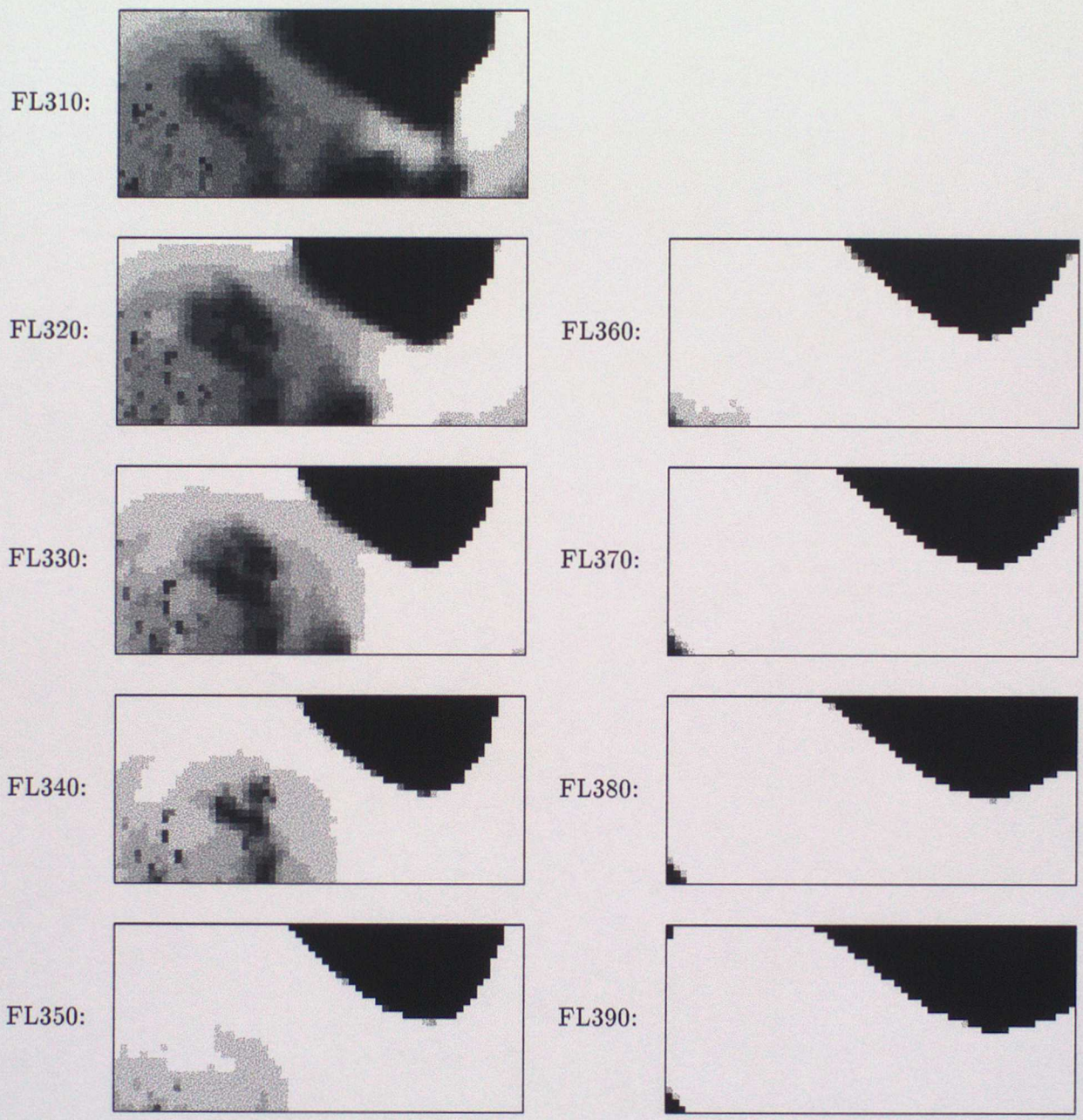

Figure 7: F00 forecasts of contrail formation for flight levels FL310 to FL390. The forecasts show the driest conditions under which contrails are forecast. White areas are where contrails are still forecast even if the relative humidity is reduced by a relative percentage of 50%. Black areas are where contrails are not forecast even if the relative humidity is increased by a relative percentage of 50%. It can be seen that at high altitudes the forecasts either predict contrail formation or no contrail formation, regardless of the relative humidity adjustment.

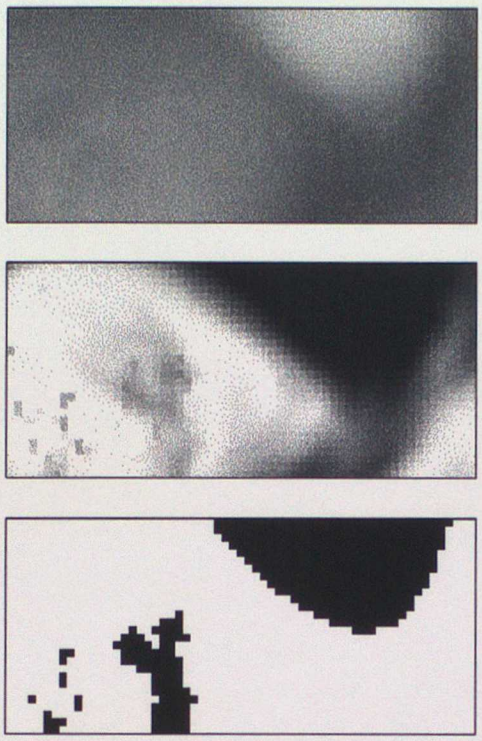

Figure 8: NWP temperature and relative humidity data at 250 hPa (approximately FL340) for the 1648 GMT satellite pass on 04 October 2000. The top image contains the temperatures (scaled dark to light from −65 to −35°C), the middle image contains the relative humidities (scaled dark to light from 0 to 100%), and the bottom image contains the contrail forecast (white for contrail formation). The upper right region is particularly warm and dry and is possibly an intrusion of stratospheric air in which contrails will not form.

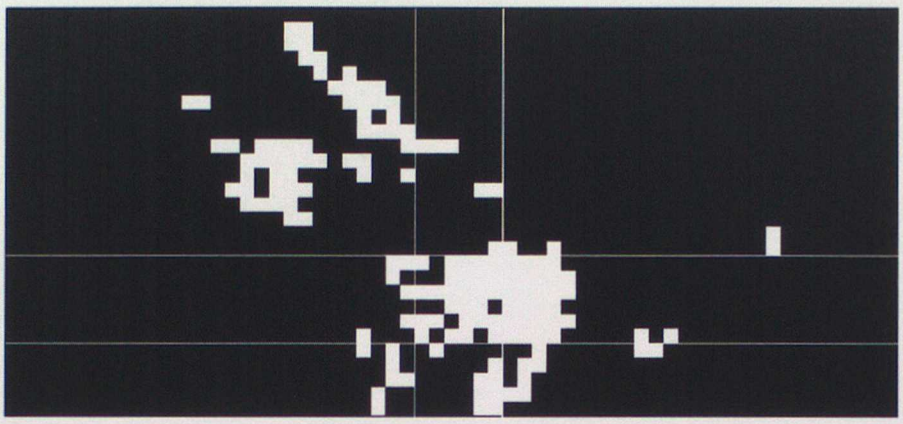

Figure 9: Detected contrails for the 1648 GMT satellite pass on 04 October 2000 mapped onto a global model grid. A global model cell is defined as a detected contrail region if the area represented by the cell contains at least one detected contrail. The outlined region corresponds to the global model cells plotted over the detected contrails in figure 2.

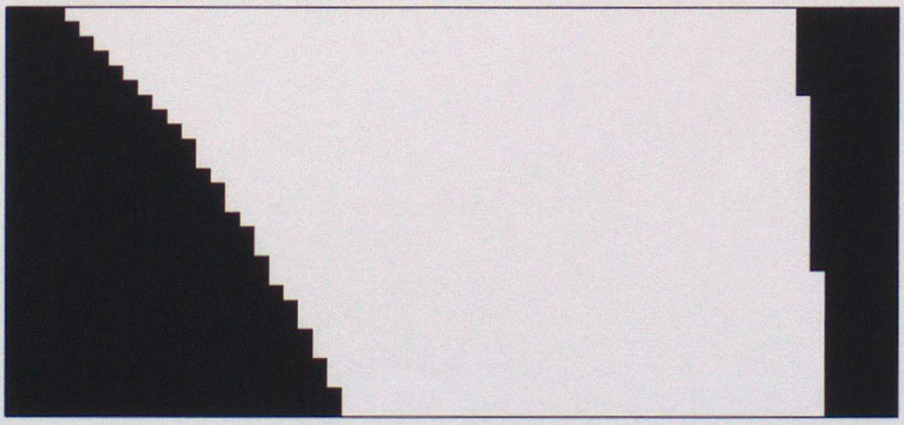

Figure 10: Detected contrail coverage for the 1648 GMT pass on 04 October 2000 mapped onto a global model grid. A global model cell is defined as a detected contrail coverage region if all the area represented by the cell has detected contrail coverage.

3.2 Expected contrail mapping

In a similar manner to the detected contrails, a global model cell was classified as an expected contrail region if any expected contrails were contained within the area represented by that cell. Since the expected contrails have known flight levels this mapping was performed for each flight level between FL310 and FL390 inclusive.

During the mapping process the expected contrails were deemed to have a half-width in the latitude direction of 0.33°, to account for aircraft latitude errors as discussed in section 2.2.5. In calculating this half-width it was assumed that if actual aircraft latitudes are normally distributed about their reported latitudes within a 3 standard deviation range of ±0.5°, then most aircraft can be expected to be within 2 standard deviations or ±0.33° of their reported latitude.

This artificial broadening of the expected contrails ensured that for a given detected contrail region there should be a corresponding expected contrail region. However it also meant that the number of expected contrail regions was overestimated, which needs to be considered when performing forecast verification.

No attempt was made to account for positional errors in the expected contrails caused by errors in the wind data used for advection. Wind induced errors are likely to be less than half the resolution of the global model (Forrester, 2001). In the latitude direction they will thus be dominated by the aircraft errors. In the longitude direction they are less important. Most aircraft over the North Atlantic fly in a roughly east-west orientation, and thus any longitude errors will only affect the endpoints of the expected contrails.

The expected contrail coverage was taken to be Shanwick airspace extended out to 40°W, as discussed in section 2.2.2. This coverage was also mapped onto the global model grid.

Expected contrails obtained from this mapping process are shown in figure 11 for the 1648 GMT satellite pass on 04 October 2000. The corresponding expected contrail coverage is shown in figure 12. Figure 11 has been masked by figure 12 so that there are no expected contrails outside the coverage area.

3.3 Removal of vertical resolution

The vertical resolution in the expected contrails and the contrail forecasts had to be removed before they could be compared with the detected contrails.

The expected contrails and contrail forecasts were first combined at each flight level, to make full use of altitude information while it was still available. At each level the contrail forecasts were masked with the expected contrails, so that only those parts of the forecasts suitable for verification purposes were retained. The masking results for the 1648 GMT pass on 04 October 2000 are shown in figure 13.

The masked forecasts were then compressed through the flight levels to remove the vertical resolution. Humidity adjustments were compared at each level for which they were available, and the one most favourable for contrail formation was selected for use. For moist atmospheres this adjustment was the largest relative amount by which the NWP relative humidity could be reduced and contrail formation still be forecast on at least one of the flight levels for which there were expected contrails. For dry atmospheres it was the smallest relative amount by which the NWP relative humidity would have to be increased before contrail formation would be forecast on at least one of these flight levels.

Figure 11: Expected contrails for the 1648 GMT satellite pass on 04 October 2000 mapped onto the global model grid for flight levels FL310 to FL390 inclusive and masked with the expected contrail coverage. For a given flight level a global model cell is defined as an expected contrail region if the area represented by the cell contains at least one expected contrail at that level.

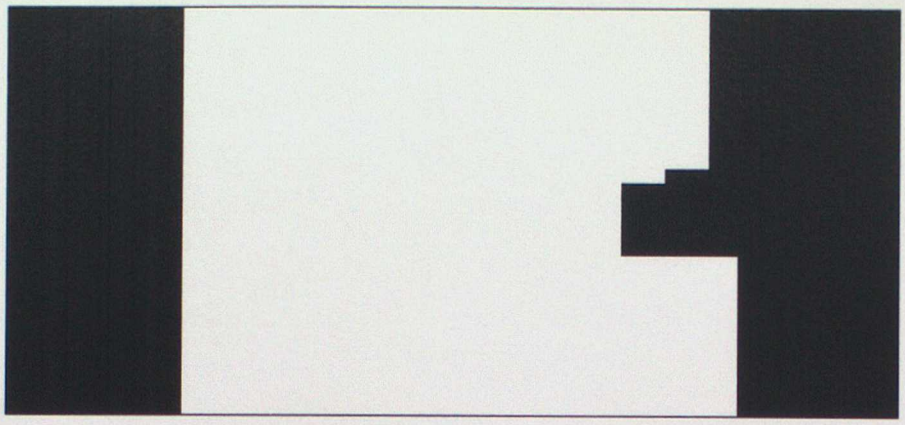

Figure 12: The area for which aircraft flight data is available, being Shanwick airspace extended out to 40°W, mapped onto the global model grid.

The only situation in which these compressed forecasts can depend on the relative humidity adjustment is when there is no intrusion of warm dry stratospheric air down through the flight levels as discussed in section 2.3.5, and no expected contrails at altitudes of approximately 250 hPa and above, where it is sufficiently cold for contrails to form regardless of the humidity, as demonstrated by table 2.

There is usually at least one expected contrail at an altitude of 250 hPa or above, as can be seen from figure 14. It is thus to be expected that the compressed forecasts will be polarised. When there is a stratospheric intrusion they will show that contrails are still not forecast even if the relative humidity data are adjusted upwards by 50%, and when there is no stratospheric intrusion they will show that contrails are still forecast even if the relative humidity data are adjusted downwards by 50%.

This polarisation can be seen in figure 15, which is the compressed forecast for the 1648 GMT satellite pass on 04 October 2000. The corresponding detected contrails are shown in figure 16. Comparison between the figures shows that, for this satellite pass at least, contrails were not detected where they were not forecast to occur.

4 Verification

Data available for forecast verification were the compressed contrail forecasts and the corresponding detected contrails. These data were available for each of the 29 satellite passes listed in table 1. Verification was performed by assessing how well the forecasts predicted the observed occurrence of contrails, relative to that which would be expected on average if there was no correlation between the contrail forecasts and the detected contrails. The assessment involved the use of contingency tables and the same method was used for each of the F00, F06, F12 and F24 forecasts. The results for the F00 forecasts are presented in detail, followed by a summary of the F06, F12 and F24 forecast results.

4.1 False alarm rate

Before performing the forecast verification it is useful to calculate the probability that a global model cell is wrongly classified as containing detected contrails. This will be called the regridded false alarm rate.

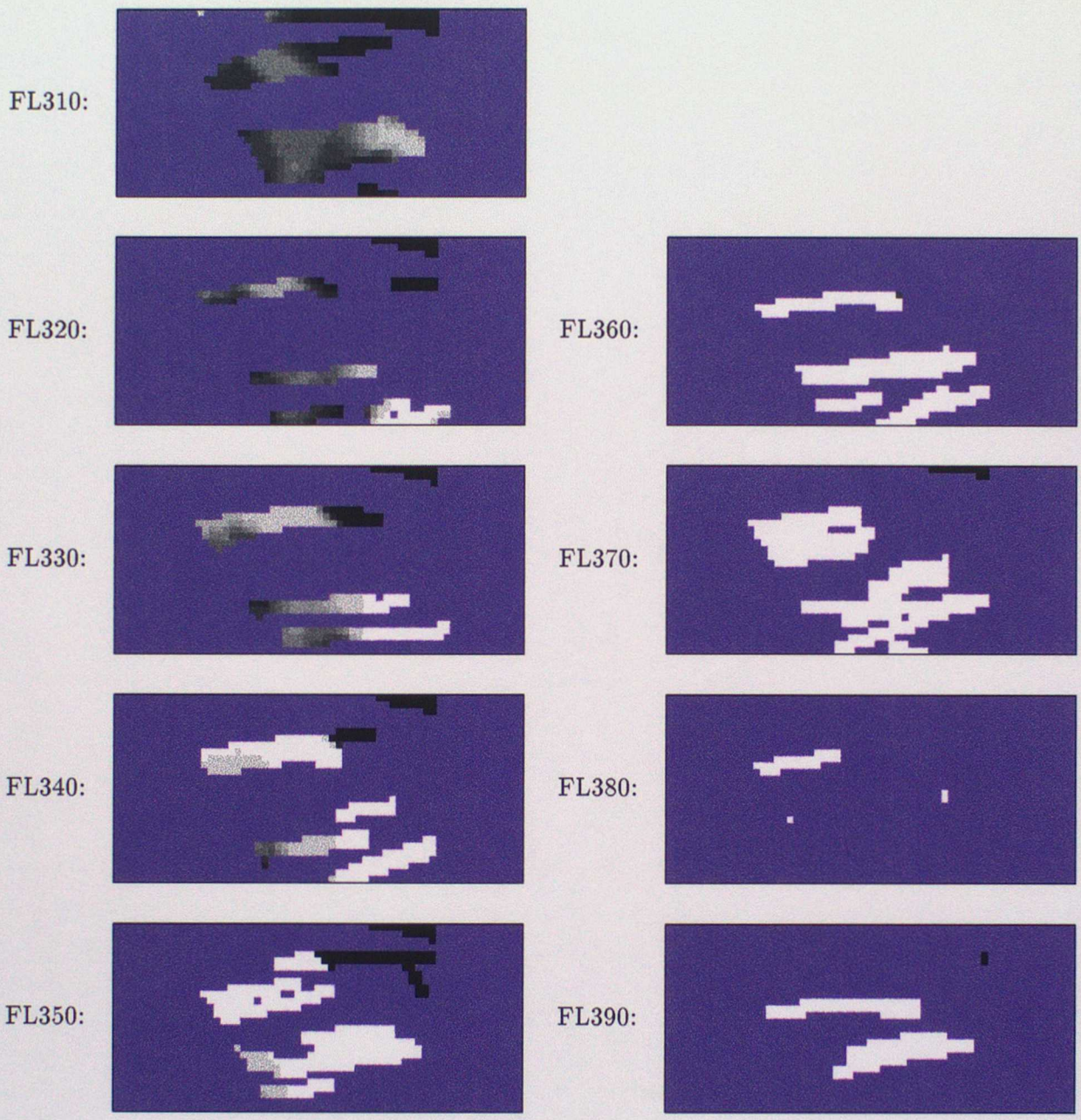

Figure 13: F00 contrail forecasts masked with detected and expected contrail coverage and the expected contrails, for the 1648 GMT satellite pass on 04 October 2000. The blue background shows where there is no detected contrail coverage (the same for each flight level) and/or no expected contrail coverage (the same for each flight level) and/or no expected contrails (different for each flight level). White areas are where contrails are still forecast even if the relative humidity is decreased by 50%. Black areas are where contrails are still not forecast even if the relative humidity is increased by 50%.

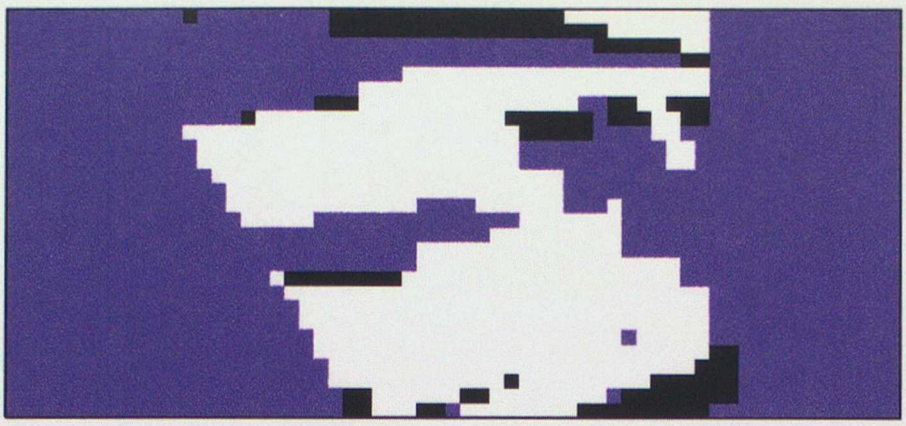

Figure 14: Maximum flight levels of the expected contrails for the 1648 GMT satellite pass on 04 October 2000. White is where the highest expected contrail is at FL340 (approximately 250 hPa) or above, while black is where the highest expected contrail is at FL330 or below. Blue is where there is incomplete data coverage and/or no expected contrails. This figure shows that there is usually an expected contrail at an altitude where it is sufficiently cold that contrails will form regardless of the relative humidity.

	Contrails detected	Contrails not detected	Total
Contrails expected	1497	12158	13655
Contrails not expected	269	3701	3970
Total	1766	15859	17625

Table 3: Contingency table for expected and detected contrails, where the expected contrails can be on any flight level between FL310 and FL390. The grand total is the number of global model cells for which there is both expected and detected contrail coverage, summed over all 29 data sets. This table can be used to calculate the false alarm rate for contrail detection after data regridding has been performed.

As discussed in section 2.1.3, the false alarm rate for contrail detection is roughly 1 AVHRR pixel in 1000, and over the North Atlantic there are approximately 3000 AVHRR pixels per global model cell. If the false alarm pixels were randomly distributed then almost every global model cell would contain detected contrails, giving a regridded false alarm rate of almost 100%. However the regridded false alarm rate should actually be somewhat lower than this, since the false alarm pixels are not randomly distributed but occur in contrail shaped groups.

The regridded false alarm rate can be calculated from the detected contrails in regions where there are no expected contrails.

A contingency table for the expected and detected contrails is given in table 3. Of the 3970 global model cells where contrails are not expected on any flight level, 269 have detected contrails. This gives a regridded false alarm rate of $(6.8 \pm 0.8)\%$, with a 2 standard deviation error. Thus for every 100 global model cells, about 7 on average will be classified as containing detected contrails purely because of the false alarm rate. This does not necessarily mean the classification will be incorrect however, because the cells could also contain actual detected contrails in addition to the false alarms.

Figure 15: F00 compressed forecast for the 1648 GMT satellite pass on 04 October 2000. White shows that at least one expected contrail is at a level where contrails are forecast to occur even if the relative humidity is reduced by a relative amount of 50%. Black shows that all expected contrails are at levels where contrails are not forecast to occur even if the relative humidity is increased by a relative amount of 50%. Blue shows incomplete data coverage and/or no expected contrails.

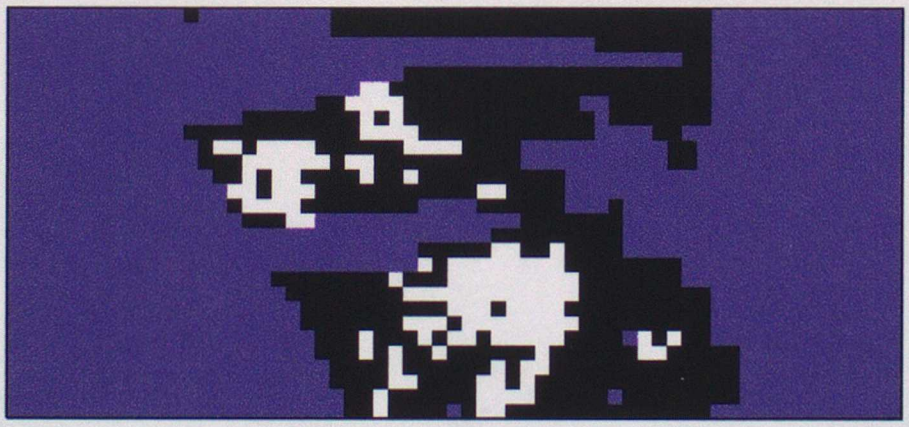

Figure 16: Detected contrails corresponding to the forecast shown in figure 15. Comparison with figure 15 shows that almost none of the detected contrails are in the regions where contrails are not forecast to occur. Detected contrails not associated with expected contrails are classified as false alarms and are not shown in this figure.

Contrails	Relative adjustment to the relative humidities (in %)										Total
	−50	−20	−10	−5	0	+5	+10	+20	+50	> +50	
Detected	1260	35	9	5	12	8	5	3	16	144	1497
Not detected	7606	234	97	53	51	49	30	61	115	3862	12158

Table 4: The observed occurrence of contrails as a function of F00 compressed forecast humidity adjustment, for all global model cells with expected contrails and both detected and expected contrail coverage.

	Forecast	Not forecast	Total
Detected	1260	144	1404
Not detected	7606	3862	11468
Total	8866	4006	12872

	Forecast	Not forecast	Total
Detected	967	437	1404
Not detected	7899	3569	11468
Total	8866	4006	12872

Table 5: Observed (top) and expected (bottom) contingency tables for the detected and forecast contrails, summed over all 29 data sets under consideration. The grand total is the number of global model cells for which the contrail forecasts were non-borderline, there were expected contrails on at least one flight level, and both expected and detected contrail coverage. The expected contingency table is calculated from the observed contingency table under the assumption that the detected contrails and contrail forecasts are independent. Comparison between the tables shows that this assumption is unlikely to be true.

4.2 F00 forecast verification

The data used for verification of the F00 forecasts are shown in table 4. This table gives the total number of global model cells with both expected contrails and full data coverage, categorised according to whether or not contrails were detected, and according to the relative humidity adjustment in the corresponding compressed contrail forecast.

The data are extremely polarised as was discussed in section 3.3, so forecast verification can only really be performed for the two situations where contrails are still forecast or still not forecast even if the NWP relative humidities are adjusted by relative amounts of plus or minus 50%. These situations will called non-borderline forecasts. A contingency table for the non-borderline F00 forecasts is given in table 5.

The observed contingency table in table 5 can be compared with that which would be expected if the detected contrails and non-borderline contrail forecasts were independent, being the expected contingency table in table 5. The χ^2 value between the observed and expected tables confirms with a high degree of certainty that there is a correlation between the detected contrails and the non-borderline contrail forecasts.

The following two sections consider the two contingency table categories that should ideally contain no data.

	Contrails forecast	Contrails not forecast	Total
Contrails detected - false alarm	230	39	269
Contrails not detected	2413	1288	3701
Total	2643	1327	3970

Table 6: Contingency table showing the relationship between the regridded false alarms and the contrail forecasts. The grand total is the number of global model cells with full data coverage but no expected contrails at any flight level. In generating this table contrails were assumed to be forecast if the F00 contrail forecasts contained a humidity adjustment of 0% or below for at least one flight level of interest.

4.2.1 Detected but not forecast contrails

An important aspect of the observed contingency table is the number of global model cells for which contrails are detected but not forecast. This number is small enough that most of the detections can be attributed to false alarms of the contrail detection algorithm.

The anticipated number of detected but not forecast contrails can be easily calculated given the regridded false alarm rate and the degree of correlation between the regridded false alarms and the contrail forecasts.

The regridded false alarm rate was calculated in section 4.1 to be (6.8 ± 0.8)%. The relationship between the regridded false alarms and the contrail forecasts is shown in table 6, from which it can be calculated that the number of regridded false alarms for which contrails are not forecast is (14.5 ± 4.3)%. This low value is unsurprising since false detections are usually cirrus cloud streaks which tend to form under similar conditions to contrails.

Of the 12872 global model cells under consideration, approximately 875 ± 100 will contain false alarms. By definition these false alarms will be among the global model cells where contrails are detected. The number of these false detections for which contrails are not forecast will be approximately 130 ± 50. This range contains the observed value of 144.

It cannot be discounted that some of the detected but not forecast contrails are due to under-forecasting by the non-borderline contrail forecasts. However the probability of correctly forecasting a contrail is likely to be well over 90%. This verifies that the non-borderline forecasts do not seriously under-forecast contrail formation, for persistent contrails at least. Furthermore if persistent contrails are not under-forecast then is unlikely that non-persistent contrails will be either, since the criterion for persistent and non-persistent contrail formation is the same.

4.2.2 Forecast but not detected contrails

A major problem with table 5 is the large number of global model cells for which contrails are forecast but not detected. There are a variety of reasons why this number is so large. The main ones are:

1. Over-estimation of the expected contrails to ensure registration between the expected and detected contrails, as discussed in section 3.2.
2. Over-forecasting of contrail formation due to incorrect conversion from relative humidity data to humidity mixing ratio data, as discussed in section 2.3.4.
3. Obscuration of contrails by cloud in the AVHRR images.

F00	Forecast	Not forecast	Total
Detected	1260	144	1404
Not detected	7606	3862	11468
Total	8866	4006	12872

F06	Forecast	Not forecast	Total
Detected	1256	156	1412
Not detected	7684	3811	11495
Total	8940	3967	12907

F12	Forecast	Not forecast	Total
Detected	1270	151	1421
Not detected	7634	3874	11508
Total	8904	4025	12929

F24	Forecast	Not forecast	Total
Detected	1280	156	1436
Not detected	7761	3799	11560
Total	9041	3955	12996

Table 7: Contingency tables for the detected and forecast contrails, summed over all 29 data sets under consideration, for the F00, F06, F12 and F24 forecasts. The grand total is the number of global model cells for which there are expected contrails on at least one flight level, and both expected and detected contrail coverage. These table show that forecasting ability does not change significantly with forecast lead time.

4. Non-persistence of contrails throughout the time windows used in calculating the expected contrails. This problem arises because the forecasts are for contrail formation only, not contrail formation and persistence.

These four reasons, and in particular the last reason, could feasibly account for all of the global model cells where contrails are forecast but not detected. However since this cannot be determined for certain no conclusions can be drawn about possible over-forecasting by the non-borderline contrail forecasts.

4.3 F06, F12 and F24 forecast verification

The observed contingency tables for the non-borderline F06, F12 and F24 forecasts are shown in table 7, together with that for the non-borderline F00 forecasts for comparison purposes. It can be seen that the contingency tables do not change significantly with forecast lead time. Any differences are probably due to those few global model cells for which conditions are borderline for contrail formation. Therefore for the non-borderline forecasts lead time does not significantly impact on forecast accuracy.

5 Conclusions

This report investigated short range contrail forecasts that could be produced by the Met Office from NWP data on an operational basis.

Verification of the forecasts proved difficult for an number of reasons, the most significant being the stacking of aircraft along North Atlantic flight routes, the false alarms of the contrail detection algorithm, and the non-persistence of contrails.

Aircraft stacking restricted forecast verification to two extreme situations: where contrails were still forecast to occur even if the NWP relative humidities were reduced by a relative amount of 50%, and where contrails were still not forecast to occur even if the NWP relative humidities were increased by a relative amount of 50%.

Borderline situations, when slight changes in the input data could alter the forecast outcome, were unable to be verified. There were very few instances of aircraft flying in conditions borderline for contrail formation, without there also being aircraft flying at other altitudes under more favourable contrail forming conditions. Additional data would be required to give sufficient numbers of these instances for verification purposes. This problem could be overcome by performing forecast verification over an area containing less air traffic.

For the non-borderline situations there were very few cases where contrails were not forecast but detected. The majority of these cases were probably false alarms of the contrail detection algorithm, so that the non-borderline forecasts probably did not under-forecast persistent contrails. It is thus likely that they also did not under-forecast non-persistent contrails, since the formation criterion for persistent and non-persistent contrails is identical.

Conversely, there were a large number of cases where contrails were forecast but not detected. This was to be expected, mainly because the forecasts were for contrail formation only, not contrail formation and persistence, but only persistent contrails were detectable in the satellite images. It is unclear whether this could account for all of the cases with forecast but not detected contrails. It thus could not be verified whether or not the non-borderline forecasts over-forecast either persistent or non-persistent contrails.

The advantage of performing verification with satellite as opposed to in-situ contrail observations was the large coverage that was readily available. However it seems that the disadvantages of this approach could outweigh its advantages, since forecasts cannot be adequately verified if the presence or absence of contrails cannot be confirmed.

To overcome the contrail detectability problems of satellite observations, the contrail prediction algorithm could be adapted to predict both contrail formation and persistence. However this could be difficult to achieve. Alternatively, contrail detections could be made using satellite images that are of sufficiently high resolution that individual aircraft are resolved. However these images may be difficult to obtain and would present data storage and processing problems.

Verification has successfully shown that the non-borderline forecasts could be reliably used to predict regions where contrails will not occur for lead times of up to 24 hours ahead. These regions would be where contrails are still not forecast to occur even if the relative humidities are increased by a relative amount of 50%, and would be sub-regions of the actual non-contrail forming regions. Such forecasts could be used by military customers to identify regions and altitudes where contrail formation is extremely unlikely to occur.

Acknowledgements

The authors would like to thank Richard Meyer and Hermann Mannstein at DLR Oberpfaffenhofen for kindly providing their contrail detection algorithm together with training in its use, and Peter Simonsson at NATS for kindly providing the Shanwick air traffic data. The authors would also like to thank two of their Met Office colleagues: Keith Whyte for assistance in setting up the AAPP software package, and Sarah Moss for discussions on the critical temperature equation.

References

Bakan, S., Betancor, M., Gayler, V., and Graßl, H. (1994). Contrail frequency over Europe from NOAA-satellite images. *Ann. Geophysicae*, 12:962–968.

Betancor Gothe, M. and Graßl, H. (1993). Satellite remote sensing of the optical depth and mean crystal size of thin cirrus and contrails. *Theor. Appl. Climatol.*, 48:101–113.

Coleman, R. F. (1996). A new formulation for the critical temperature for contrail formation. *J. Appl. Meteorol.*, 35:2270–2282.

Engelstad, M., Sengupta, S. K., Lee, T., and Welch, R. M. (1992). Automated detection of jet contrails using the AVHRR split window. *Int. J. Remote Sensing*, 13(8):1391–1412.

Forrester, D. (2001). Private communication.

Gerz, T., Dürbeck, T., and Konopka, P. (1998). Transport and effective diffusion of aircraft emissions. *J. Geophys. Res.*, 103(D20):25905–25913.

Gierens, K., Sausen, R., and Schumann, U. (1999). A diagnostic study of the global distribution of contrails. Part II: Future air traffic scenarios. *Theor. Appl. Climatol.*, 63:1–9.

Jackson, A., Newton, B., Hahn, D., and Bussey, A. (2001). Statistical contrail forecasting. *J. Appl. Meteorol.*, 40(2):269–279.

Jensen, E. J., Toon, O. B., Kinne, S., Sachse, G. W., Anderson, B. E., Chan, K. R., Twohy, C. H., Gandrud, B., Heymsfield, A., and Miake-Lye, R. C. (1998). Environmental conditions required for contrail formation and persistence. *J. Geophys. Res.*, 103(D4):3929–3936.

Kärcher, B., Busen, R., Petzold, A., Schröder, F. P., and Schumann, U. (1998). Physicochemistry of aircraft-generated liquid aerosols, soot, and ice particles. 2: Comparison with observations and sensitivity studies. *J. Geophys. Res.*, 103(D14):17129–17147.

Lee, T. F. (1989). Jet contrail identification using the AVHRR infrared split window. *J. Appl. Meteorol.*, 28(9):993–995.

Mannstein, H., Meyer, R., and Wendling, P. (1999). Operational detection of contrails from NOAA-AVHRR-data. *Int. J. Remote Sensing*, 20(8):1641–1660.

Meyer, R. (2000a). Private communication.

Meyer, R. (2000b). *Regionale Kondensstreifen-Bedeckung aus Satellitendaten und ihr Einfluss auf den Strahlungshaushalt.* PhD thesis, Universität München.

Moss, S. J. (1999). The testing and verification of contrail forecasts using pilot observations from aircraft. *Meteorol. Appl.*, 6:193–200.

Peters, J. L. (1993). New techniques for contrail forecasting. Technical Report AWS/TR–93/001, Air Weather Service.

Schrader, M. L. (1997). Calculations of aircraft contrail formation critical tmeperatures. *J. Appl. Meteorol.*, 36(1725–1729).

Schumann, U. (1996). On conditions for contrail formation from aircraft exhausts. *Meteorol. Z.*, 5(1):4–23.

Schumann, U., Busen, R., and Plohr, M. (2000). Influence of propulsion efficiency on contrail formation: Theory and experimental validation. Technical Report 139, Institut für Physik der Atmosphäre, Deutsches Zentrum für Luft- und Raumfahrt, DLR Oberpfaffenhofen.

Walters, M. K. and Shull, J. D. (1999). A validation study of the Air Force Weather Agency (AFWA) JETRAX contrail forecast algorithm. In *Eighth Conference on Aviation, Range, and Aerospace Meteorology*, pages 591–598. American Meteorological Society.

A Acronyms

AAPP	ATOVS and AVHRR Processing Package
AVHRR	Advanced Very High Resolution Radiometer
ATOVS	Advanced TIROS Operational Vertical Sounder
EUMETSAT	European Organisation for the Exploitation of Meteorological Satellites
ICAO	International Civil Aviation Organisation
MOD	Ministry of Defence
NATS	National Air Traffic Services
NOAA	National Oceanic and Atmospheric Administration
NWP	Numerical Weather Prediction

Investigation into the use of Meteosat water vapour channel data in contrail forecasting

F I Hilton

November 2001

Abstract

The accuracy of forecasts of contrail formation depends on the accuracy of the meteorological data that is used to create the forecasts. Any errors in the Numerical Weather Prediction (NWP) humidity data will be passed through to the forecast. This report considers data sources which could be incorporated into the NWP model to improve relative humidity fields at aircraft flight levels and thus the forecasting of contrails. Incorporation of Meteosat and Meteosat Second Generation Water Vapour channel data are considered in more detail through a 1D-var information content study. The results of this study suggest that these data will not lead to an appreciable improvement in forecast accuracy using currently available data assimilation techniques.

1 Introduction

Previous research has shown that the success of mathematical models of contrail formation depend critically on the accuracy of the meteorological data used (Jackson et al., 2001). Contrails form when water vapour in the exhaust of the aircraft condenses and freezes on mixing with the ambient air (Schumann, 1996). The ability to forecast contrails thus depends on knowing the atmospheric conditions in both the aircraft exhaust and the ambient air, as well as on having an equation to represent the mixing process accurately. The requirement for accurate data means that forecasting contrails is difficult, particularly if conditions are borderline for formation.

Section 2.3.4 of Part A discusses the dependence of the critical temperature T_c, above which contrails will form, on ambient temperature and relative humidity. It shows that when conditions become borderline for contrail formation, errors in the relative humidity can easily alter the forecast outcome.

It is difficult to quantify the error in NWP relative humidity as this ideally requires an independent set of measurements with greater accuracy than the NWP forecast. Verification programs have shown that NWP short-range forecast relative humidity fields for the upper troposphere are biased with respect to radiosonde measurements by up to 10%, and have an average root mean square error of up to 25% (Forrester, 2001). This could suggest that an adjustment to the forecast might improve the forecasting of contrails. However, these statistics could be the result of bias in the radiosonde measurements rather than in the NWP model: radiosonde measurements are known to be less accurate higher in the atmosphere. The variability between the two measurements will also be affected by the different volumes of atmosphere represented by the NWP grid point and the radiosonde measurement.

The sensitivity of the forecast to relative humidity and the possibility of bias in the NWP data prompted an investigation into methods of increasing the accuracy of the NWP humidity profile. One method of doing this is to use observational data (for example, satellite data) to nudge the profile. Some of the sources of data that could be used for this purpose are discussed in Section 2.

2 Sources of Humidity Data

There are three main sources of relative humidity information: NWP models, satellite radiances and radiosonde measurements. If the information is to be used for forecasting contrails, even at short range, it seems unlikely that the reliance on NWP data will be removed. The NWP forecast is likely to be the best guess of the atmospheric state at the time for which the forecast is valid. However, observations are an important source of information and provide stability to the NWP model. Some sources of humidity observations are discussed here.

Radiosonde observations are limited in their use for the North Atlantic area, as they are typically land-based instruments. Despite the advantage they hold in that they measure an atmospheric profile, they do not have the spatial coverage that satellite data have and also lack the temporal resolution of some satellites. The accuracy of radiosonde measurements of upper tropospheric humidity is also questionable. Satellite data is preferable in many ways for this type of study, where a broad area is under consideration.

Satellite data used in humidity estimation generally come from sounding instruments on polar orbiting satellites. Currently the only infrared sounding data incorporated into the Met Office NWP model is the three channel HIRS data available every 12 hours. Future instruments will provide more detailed information, such as the high spectral resolution AIRS instrument due to be launched on NASA's Aqua platform in the near future.

Being infrared sounders, HIRS and AIRS, like Meteosat, are unusable in areas of cloud. Microwave sounding instruments, such as the AMSU-B instruments on recent NOAA platforms, also provide humidity data. AMSU-B data (3 channels) have recently been incorporated into the Met Office NWP model as well as the HIRS data. One advantage of microwave instruments is that they can provide information below regions of cloud, although more research is needed before cloud-contaminated information can be incorporated. An AMSU instrument will also fly on the Aqua platform along with another microwave humidity profiler, HSB. Together the instruments on Aqua will provide a wealth of humidity profile information.

One additional source of satellite data which could be useful is Meteosat, the geostationary weather satellite operated by EUMETSAT. The advantage of Meteosat data is that the imagery is available hourly via the Autosat system. Although Meteosat is not a sounding instrument (i.e. it has only one water vapour-sensitive channel), the spatial and temporal resolution of the data are good. In simple terms, the more channels of differing wavelengths that a satellite instrument has, the more information about the vertical distribution of relative humidity its measurements contain. The Meteosat Water Vapour (WV) channel is centred on 6.3 μm, coinciding with a water vapour absorption band. The radiance measured by this channel is thus related to the water vapour content of the atmosphere from approximately 250 to 600 hPa and can be used to provide information on layer average relative humidity. Meteosat Second Generation (MSG) is to be launched in the near future. MSG has two water vapour channels at 6.2 μm and 7.3 μm.

The main flight levels of transatlantic commercial aircraft correspond to a pressure range of approximately 300 to 200 hPa and figure 7 in Part A shows that the forecasts are extremely variable between different flight levels. The lack of information on the vertical distribution of water vapour

in the Meteosat radiances is therefore a drawback. However, owing to the advantages of the timeliness and frequency of Meteosat data, a study was carried out into the effect of its assimilation on the forecasting of contrails.

3 Assimilation of Meteosat/MSG data

The Autosat data covers the study area at a spatial resolution of approximately 5km and is calibrated to 1K brightness temperature resolution. Two methods of integrating Meteosat/MSG WV imagery were considered:

1. Convert the satellite radiance measurement into an estimate of relative humidity using a method based on simplified Radiative Transfer (RT) modelling. Compare this with a weighted average of the NWP data over the layers corresponding to the WV channel sensitivity.
2. Predict the radiance measurement that would result from the NWP model fields using RT modelling. Compare this simulated radiance with the Meteosat measurement and calculate the optimum adjustment to the model with Variational Analysis.

The first method is based on that of Soden and Bretherton (1993). Although it is computationally straightforward, it has several drawbacks. The relationship between brightness temperature and relative humidity is derived from RT theory, but once the form of the equation is defined, regression is used to calculate the coefficients. The method is thus semi-empirical and ideally a large amount of independent data is needed to determine the constant terms. A further problem is that the sensitivity of the satellite to water vapour at different depths depends upon the atmospheric profile. If the humidity is high in the upper atmosphere the satellite will not 'see' humidity lower down. It is not easy to account for this effect using the first method as the RT equations used assume a standard atmospheric profile. The method has a further major drawback: once the satellite relative humidity has been compared to the column weighted average of the NWP fields, it is not clear how to assign any necessary layer average correction across the different model levels.

The second method is more theoretically sound and it produces an adjustment which is physically appropriate and consistent with other model fields. Variational analysis calculates the optimum correction to the model needed to take account of the new data (i.e., the Meteosat/MSG measurements). One clear advantage over the first method is that the simulation of a radiance measurement from the NWP profile incorporates information on the atmospheric conditions. The optimisation of the adjustment then takes into account the relative errors between the model and the satellite measurement. This ensures that a good model will not be adversely affected by bad data, although undetected global bias in the data (or model) may prevent full optimisation. This method is computationally more expensive, even if only a column of atmosphere is considered, i.e. a simplification of the three dimensional variational analysis (3D-var) problem to one dimension (1D-var).

4 Meteosat WV information content study

An information content study was carried out using methodology similar to Eyre (1990) to determine whether the assimilation of Meteosat/MSG data under 1D-var would yield any improvement to the contrail forecasts via the NWP humidity fields. Meteosat is not an ideal instrument to provide information on humidity profiles, as it has only one water vapour-sensitive waveband and can therefore provide only a layer-average estimate of water vapour. It is possible that improvement of the column-integrated water vapour would improve the measurement on particular levels as

well. This can be tested by performing a comparison between the background state (i.e., the NWP model first guess) and the analysed state (i.e., the model plus the adjustment made under 1D-var) on model levels. MSG is expected to have greater skill at assigning water vapour to particular levels since it has two water vapour channels (Channels 2 and 3).

It is possible to estimate the error variance of a 1D-var analysis without performing a full optimisation of the corrections. By looking at the retrieval error of the relative humidity at different pressures, it is possible to determine whether the inclusion of Meteosat/MSG data would cause a useful reduction in error at the flight levels under consideration. Note that this method assumes that there is no bias between the background field and the satellite observation, although continuous monitoring of 1D-var may allow identification of any bias that does exist.

4.1 Information content study – theory

First the background (model) error covariances must be defined. In this case, error covariances related to temperature were ignored since the error in humidity dominates the error in forward modelled water vapour channel radiances. A matrix known as **B** represents the covariance, σ_{ij}^2, between specific humidity at pressure level i and specific humidity error at pressure level j. The diagonal elements of this matrix, σ_{ii}^2, represent the variance of the model humidity error at each pressure level – the quantity which incorporation of the Meteosat data is hoped to reduce:

$$\mathbf{B} = \begin{pmatrix} \sigma_{11}^2 & \sigma_{12}^2 & \cdots \\ \sigma_{21}^2 & \sigma_{22}^2 & \cdots \\ \vdots & \vdots & \vdots \end{pmatrix} \tag{1}$$

The aim of the information content study was to generate a matrix whose elements represented the error covariances after incorporation of the satellite data (i.e., the analysed state). This matrix, **A**, contains the expected values of the error covariances of the best linear unbiased estimator of the true atmospheric state:

$$\mathbf{A} = (\mathbf{B}^{-1} + \mathbf{H}^T\mathbf{R}^{-1}\mathbf{H})^{-1} \tag{2}$$

H is the gradient of the observation operator and relates changes in specific humidity in the atmosphere to changes in brightness temperature. **R** is the observation error covariance matrix and combines the measurement error of the observation with the RT forward modelling error. The standard deviation of the combined measurement and forward modelling error, i.e., the value that was squared to create the leading diagonal of **R**, is referred to hereafter as the observation error.

Matrix **A** is of the same form as **B**, and the leading diagonal elements represent the post-adjustment specific humidity error variances at each atmospheric model level.

If any value of the leading diagonal of **A** is less than the corresponding value of **B**, then the inclusion of Meteosat data is likely to cause an improvement in water vapour retrieval at that level. The improvement can be quantitatively expressed though **A** – **B**. An improvement to the layer precipitable water can also be calculated by summing over a pressure range.

4.2 Information content study – method

The matrix **A** was calculated according to Equation 2. **H** was calculated using the program RTTOV-6 (Saunders et al., 1999). RTTOV-6 uses an atmospheric profile and the characteristics of the satellite instrument to calculate a simulated brightness temperature. It also calculates the

gradient of the simulated brightness temperature with respect to changes in humidity at each model level. The matrix of gradients expressed at each model level is essentially a weighting function, and defines **H**. The calculation was performed on 43 levels, from 0.10 to 1013.25 hPa.

The atmospheric profiles used as input were generated from ECMWF model profiles on 50 atmospheric levels and interpolated to the 43 RTTOV-6 model levels. A range of profiles were selected from within the North Atlantic study area. The results in section 4.3 are presented for a North Atlantic profile with moderate humidity levels (see figure 1). An alternative would have been to use profiles derived from radiosonde measurements but these did not extend above an altitude of 300 hPa, the lowest pressure level studied for contrail forecasts.

The background error matrix was provided on 26 model levels corresponding to pressures from 122.04 to 1013.25 hPa. The study was therefore limited to this pressure range but the water vapour content of the atmosphere above this level is in any case extremely low. The matrix was adapted for 1D-var from the 3D-var matrix by averaging over the Northern Hemisphere and interpolating to the RTTOV model levels (Poulsen, 2001). The 3D-var covariances are derived from the differences between T+24 and T+48 operational forecasts (valid at the same time) accumulated over 28 days (Ingleby, 2001).

The error variance used in **R** was initially taken as $2\,\mathrm{K}^2$. Meteosat WV channel is similar in its wavelength to HIRS Channel 12. The RTTOV-6 Science and Validation Report (2000) shows that the forward modelling error standard deviation for HIRS 12 with respect to a full line-by-line calculation is 0.75 K, and a similar value was deemed appropriate for Meteosat WV. The report also gives the noise equivalent brightness temperature for HIRS 12 as 1K. Combined, this would give an error variance for HIRS 12 of $1.56\,\mathrm{K}^2$. This was increased to $2\,\mathrm{K}^2$ for the initial trial with Meteosat, giving an observation error of $\sqrt{2}$ K. HIRS 12 is assimilated operationally using 3D-var assuming an observation error of 4 K, and so another trial was run using 4 K instead of $\sqrt{2}$ K. An observation error of 0.4 K is used in preprocessing of HIRS data, and this level of accuracy was also investigated. The same values were used for the two channels of MSG.

4.3 Information content study – results

The results of this study are presented in such a way as to compare the potential value of assimilating Meteosat WV information with the potential value of HIRS data. Results are given in terms of retrieval uncertainty, i.e. $\sqrt{\mathbf{A}_{ii}}$. A further comparison was made with the assimilation of the two water vapour channels of Meteosat Second Generation (MSG). A zenith angle of 40° was used for Meteosat and MSG, as this roughly corresponds to the minimum zenith angle in the Meteosat data covering the North Atlantic study area. Tests for HIRS were carried out at two zenith angles of 0° and 40°.

Two measures of the improvements following satellite data assimilation are provided. The first is an estimate of the uncertainty in column-integrated total precipitable water over a layer between 122.04 and 436.95 hPa. This calculation sums over the levels which correspond the closest to the pressures at which contrail forecasts were generated. This measure is expressed as a proportion of the layer precipitable water. This calculation was performed for Meteosat, MSG, HIRS and also for Meteosat plus HIRS together and MSG plus HIRS. Since HIRS data is already assimilated into the model, it was important to gauge what potential Meteosat WV or MSG has on top of the HIRS data already incorporated. Meteosat was not expected to add much improvement, as its weighting function is very similar to HIRS channel 12. These results are presented for observation errors of 0.4, $\sqrt{2}$ and 4 K in table 1.

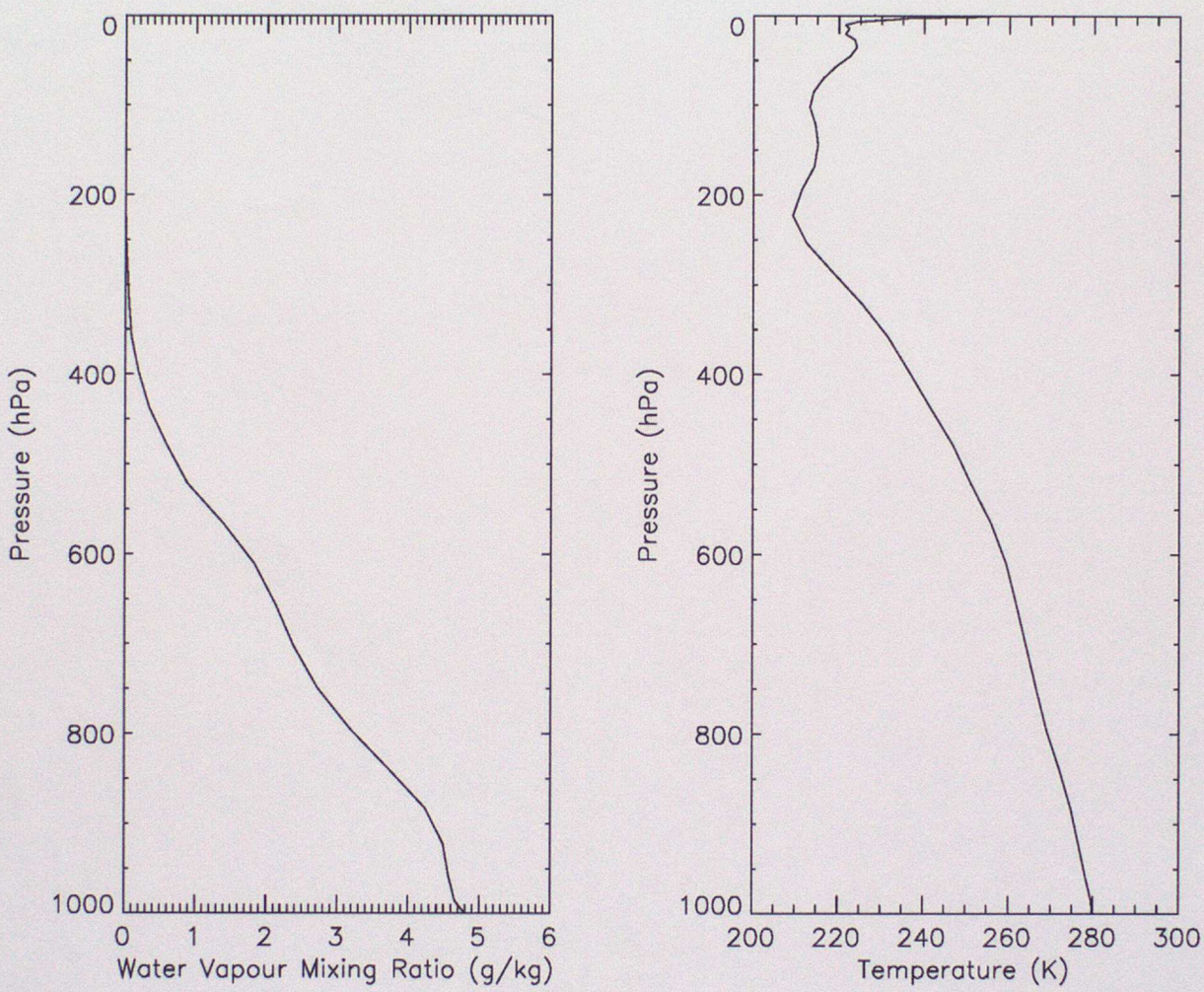

Figure 1: Atmospheric profile used to generate the gradient matrices **H** for which the results are presented in section 4.3

Satellite Observation Assimilated	Observation Error		
	0.4	$\sqrt{2.0}$	4.0
Background	**0.236**	**0.236**	**0.236**
HIRS 10,11,12 at Zenith 40	0.132	0.166	0.213
HIRS 10,11,12 at Zenith 0	0.136	0.168	0.215
MSG 2,3 at Zenith 40	0.136	0.169	0.213
Meteosat WV at Zenith 40	**0.162**	**0.184**	**0.220**
HIRS 12 at Zenith 40	0.159	0.182	0.219
MSG 2 at Zenith 40	0.167	0.186	0.220
HIRS 10,11,12 Zen.40 + Meteosat Zen.40	0.132	0.160	0.204
HIRS 10,11,12 Zen.0 + Meteosat Zen.40	0.136	0.162	0.205
HIRS 10,11,12 Zen.40 + MSG 2,3 Zen.40	0.126	0.155	0.199

Table 1: Standard deviation of column-integrated water vapour retrieval error over pressure range 122.04 hPa to 436.95 hPa expressed as proportion of column total water vapour.

Although the error in layer precipitable water gives some indication of the potential for the satellite instrument to reduce the error in upper tropospheric humidity, the large variability of the contrail forecasts with pressure means that it is important to be able to assign the water vapour accurately to different model layers. Meteosat was expected to have less skill in this than HIRS or MSG, since it has only one water vapour-sensitive channel. The uncertainty in the water vapour mixing ratio on individual model levels provides the second measure of improvement and is shown in figures 2 to 5 to determine the relative skills of Meteosat, MSG and HIRS. The error in the natural logarithm of the water vapour mixing ratio is also shown on model levels, as this demonstrates the errors in the upper levels of the atmosphere more clearly. This measure is also closely related to the error in relative humidity if the temperature error is neglected.

The information in table 1 shows that the assimilation of Meteosat WV channel observations will do less to reduce the retrieval uncertainty of column-integrated water vapour than the assimilation of all three HIRS channels or the two MSG channels. Meteosat WV will reduce the error a comparable amount to HIRS 12 or MSG 2 alone. Assimilation of Meteosat and HIRS together allows a further small reduction in the retrieval error over assimilation of the HIRS channels only. MSG and HIRS together provide the best error reduction.

The results are not greatly sensitive to the HIRS viewing angle. However, the sensitivity to observation error is greater. With the observation error set at the level used currently in operational HIRS assimilation, 4 K, the reduction in retrieval error following assimilation of any of the satellite data is a maximum of 10% of the background. Assuming an observation error of 0.4 K, the reduction is more significant at around 40% of the background error. At this low observation error, the assimilation of Meteosat WV channel information as well as the HIRS channels does not result in any improvement over HIRS alone. This suggests that the improvement seen at $\sqrt{2}$ and 4 K is a result of the statistical benefit of having more observations where the accuracy of the observations is lower.

Figures 2, 3 and 4 show the improvements to the uncertainty in water vapour on individual model levels after satellite data assimilation with observation errors of $\sqrt{2}$, 4 and 0.4 K respectively. It is clear that the HIRS assimilation has the greatest overall impact on the retrieval error, but that the benefits are mostly at the lower levels. Figure 3 shows that with an observation error of 4 K none of the satellites individually cause much improvement to the water vapour retrieval for individual layers.

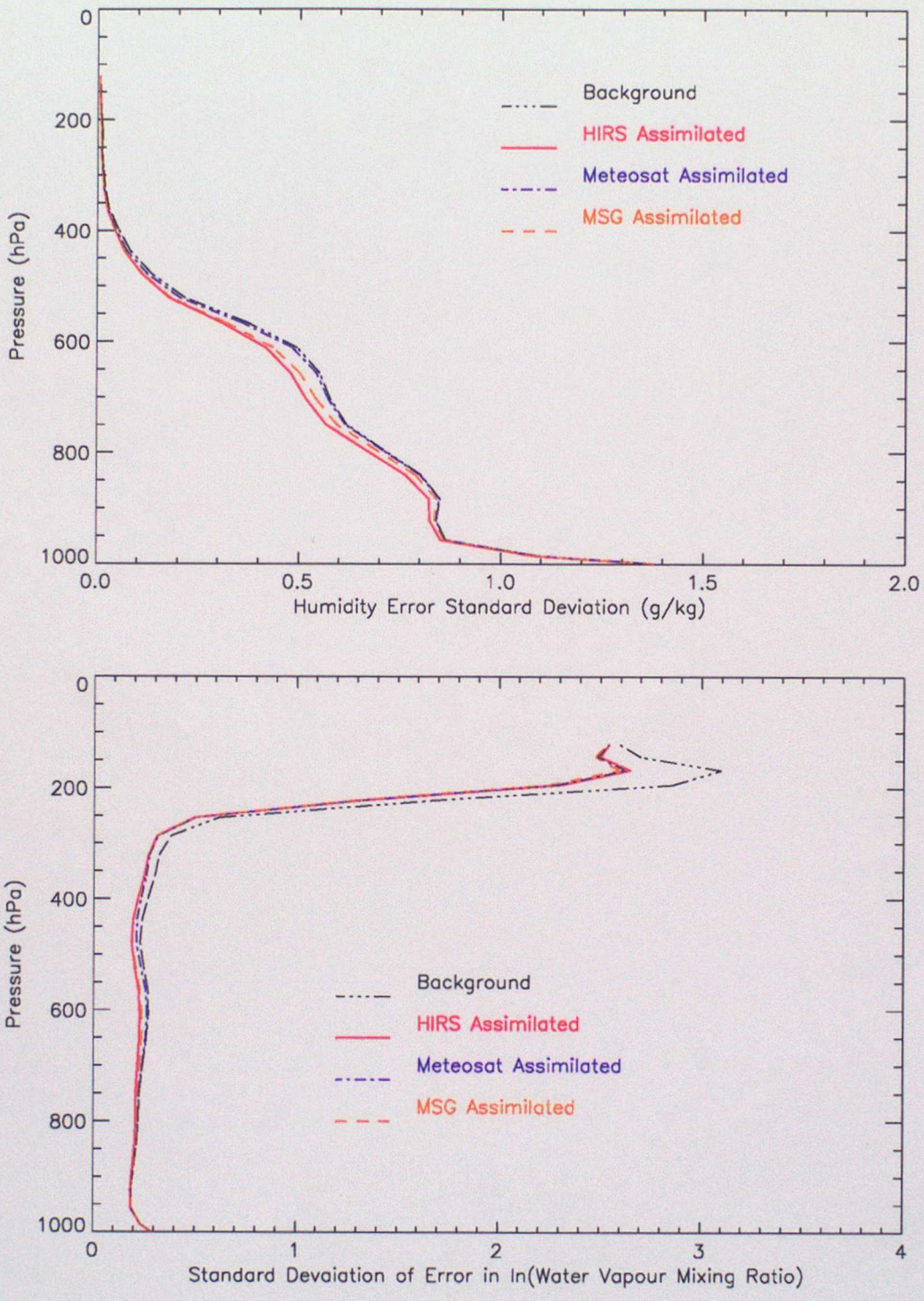

Figure 2: Water vapour mixing ratio retrieval error for assimilation of HIRS, Meteosat and MSG with observation error of $\sqrt{2}$ K. Top graph shows standard deviation of error in water vapour mixing ratio, bottom graph shows error in natural logarithm of water vapour mixing ratio which shows the errors in the upper atmospheric water vapour more clearly.

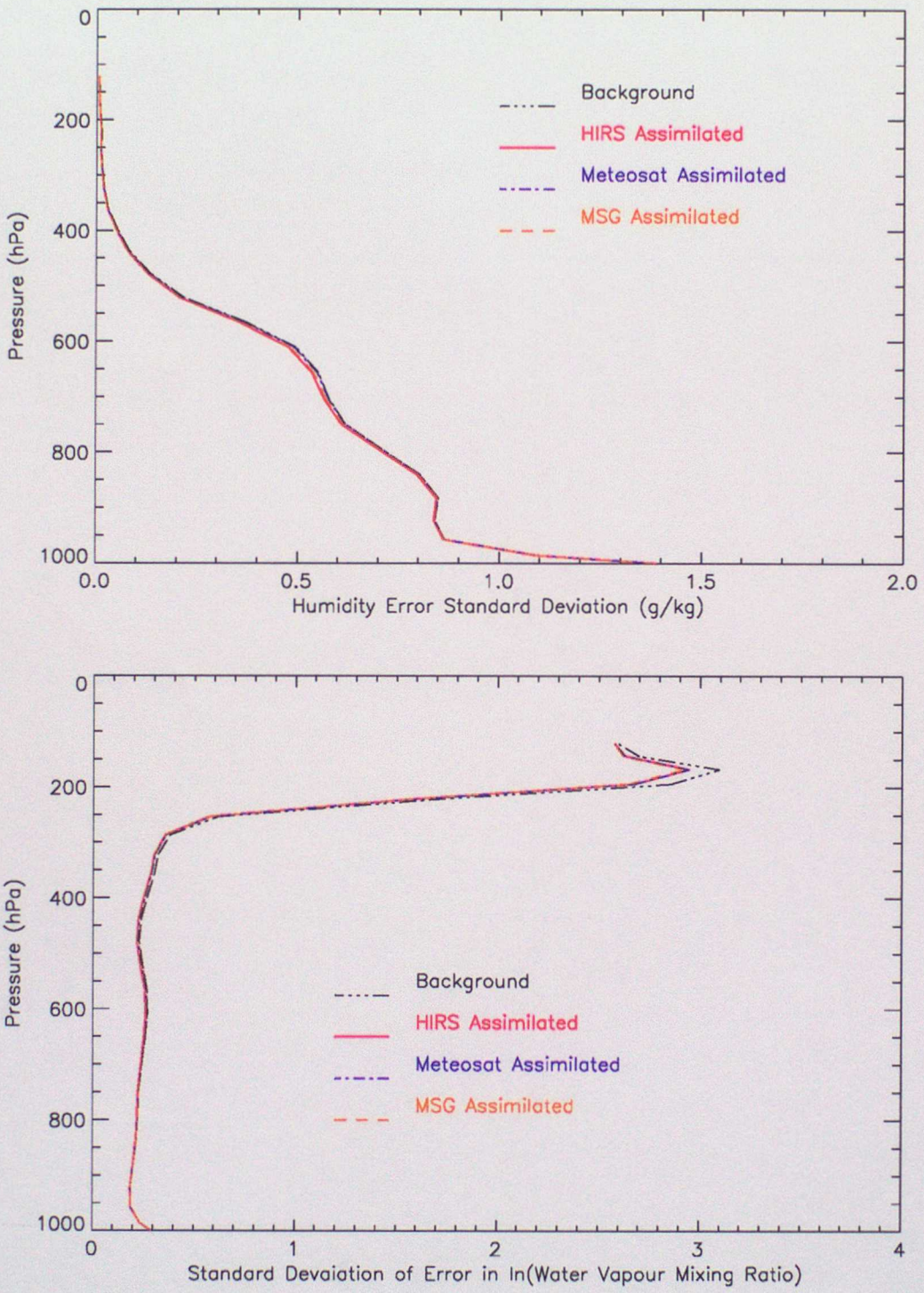

Figure 3: As figure 2 but with an observation error of 4K.

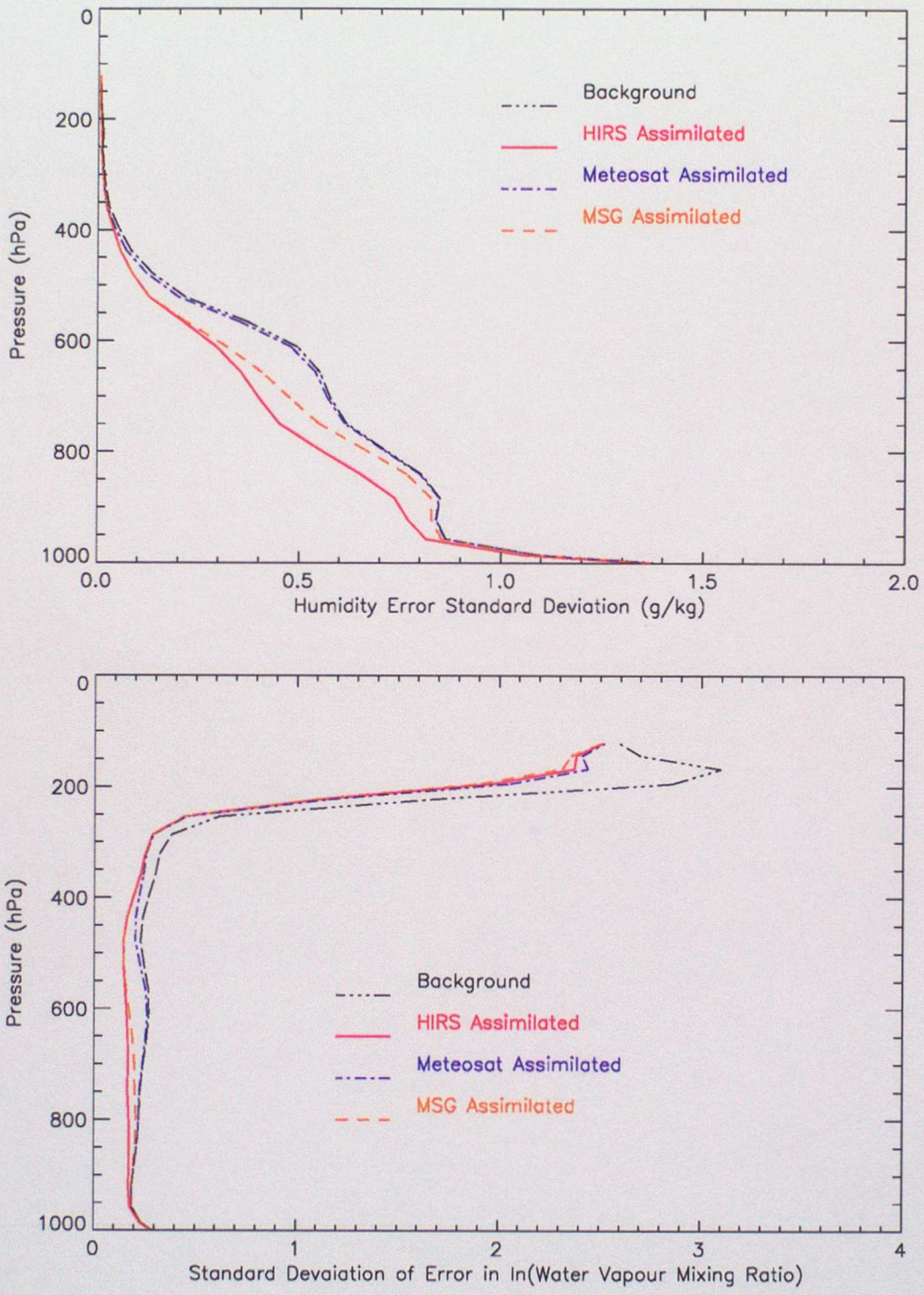

Figure 4: As figure 2 but with an observation error of 0.4K.

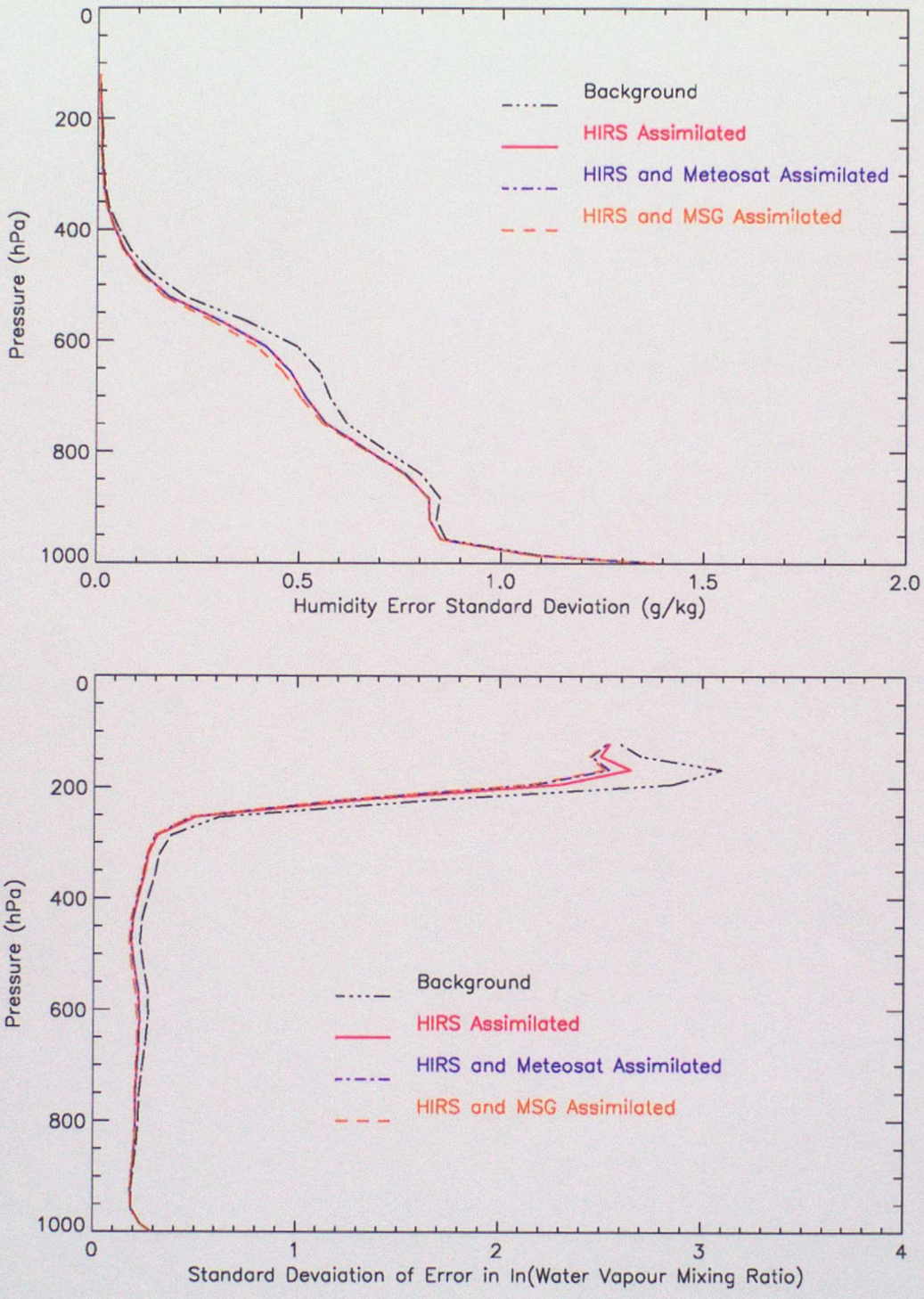

Figure 5: As figure 2, with observation error of $\sqrt{2}$K, but comparing the retrieval error following assimilation of HIRS and Meteosat/MSG together with the assimilation of HIRS alone.

Figure 4 is perhaps a better indication of the information potentially available in the satellite data since the observation error is low. However, it should be noted that 0.4 K is not an appropriate observation error for Meteosat if the Autosat data is to be used, since the calibration of this data source is only to within 1K. This figure shows the benefit of the increased number of water vapour-sensitive channels in MSG and HIRS when the satellite data and RT modelling are considered accurate. Meteosat is much less able to reduce the retrieval error, especially below 400 hPa. From the point of view of contrail forecasting, this result does not rule out the possibility that Meteosat WV may be of use in improving the precision of modelled water vapour, since 400 hPa is below the minimum altitude at which forecasts are produced.

At pressures less than 400 hPa, the quantity of water vapour in the atmosphere is much lower than at higher pressures, resulting in much larger uncertainties (visible in the graphs of the error in the natural logarithm of water vapour mixing ratio. At these pressures the performance of Meteosat is more comparable to that of MSG or HIRS.

Figure 5 compares the assimilation of HIRS and Meteosat/MSG together with the assimilation of HIRS alone, assuming an observation error of $\sqrt{2}$K. This gives an indication of the improvement to the model water vapour channels that will be possible if Meteosat or MSG is assimilated with a moderate observation error, given that HIRS data is already assimilated. There is little difference in the reduction of the retrieval error between these three scenarios. Assimilating data from HIRS and Meteosat provides a slight improvement in the retrieval error over HIRS alone above 200 hPa. The assimilation of Meteosat data may thus provide some small benefit to the prediction of water vapour mixing ratio at these pressures through the assimilation of a more up-to-date measurement. However, since the quantity of water vapour is very small at these levels, the adjustments would also be very small. The further improvement with MSG is not much greater. These results suggest that the impact on the contrail forecasts will be negligible since, at these pressures, contrails are forecast even at extremely low relative humidities (see Part A, section 2.3.4). The impact on contrail forecasts is discussed further in section 5.

5 The effect of Meteosat assimilation on contrail forecasting

The results of the information content study suggest that assimilation of Meteosat data would have little impact on the accuracy of the contrail forecasts. The weighting function of the WV channel means that Meteosat has little potential to reduce the uncertainty in upper tropospheric humidity in the presence of HIRS (see figure 4). After assimilation of HIRS, the maximum further improvement to any layer that Meteosat gives is 6.4% of the background retrieval error at 167.95 hPa (assuming an observation error of $\sqrt{2}$ K). The further improvement to column-integrated water vapour mixing ratio is 2.5% of the background uncertainty. These adjustments are small, and it is unlikely that the gain in accuracy of the contrail forecasts would merit the assimilation of Meteosat data. MSG gives similar results, with a maximum improvement of 7.2% of the background uncertainty at 167.95 hPa and 4.7% for the integrated column.

To test the impact of the satellite data assimilation, the effect of the uncertainty in water vapour mixing ratio on the calculation of the critical temperature for contrail formation was assessed. A base relative humidity of 50% and ICAO standard temperatures were assumed between pressures of 150 and 400 hPa. The relative humidity, after conversion to water vapour mixing ratio, was adjusted by the retrieval errors before and after satellite assimilation (see figure 5). Four levels of error were tested: the background value, the error after assimilation of HIRS alone, the error after assimilation of HIRS and Meteosat WV, and the error after assimilation of HIRS and MSG. An observation error of $\sqrt{2}$ K was assumed.

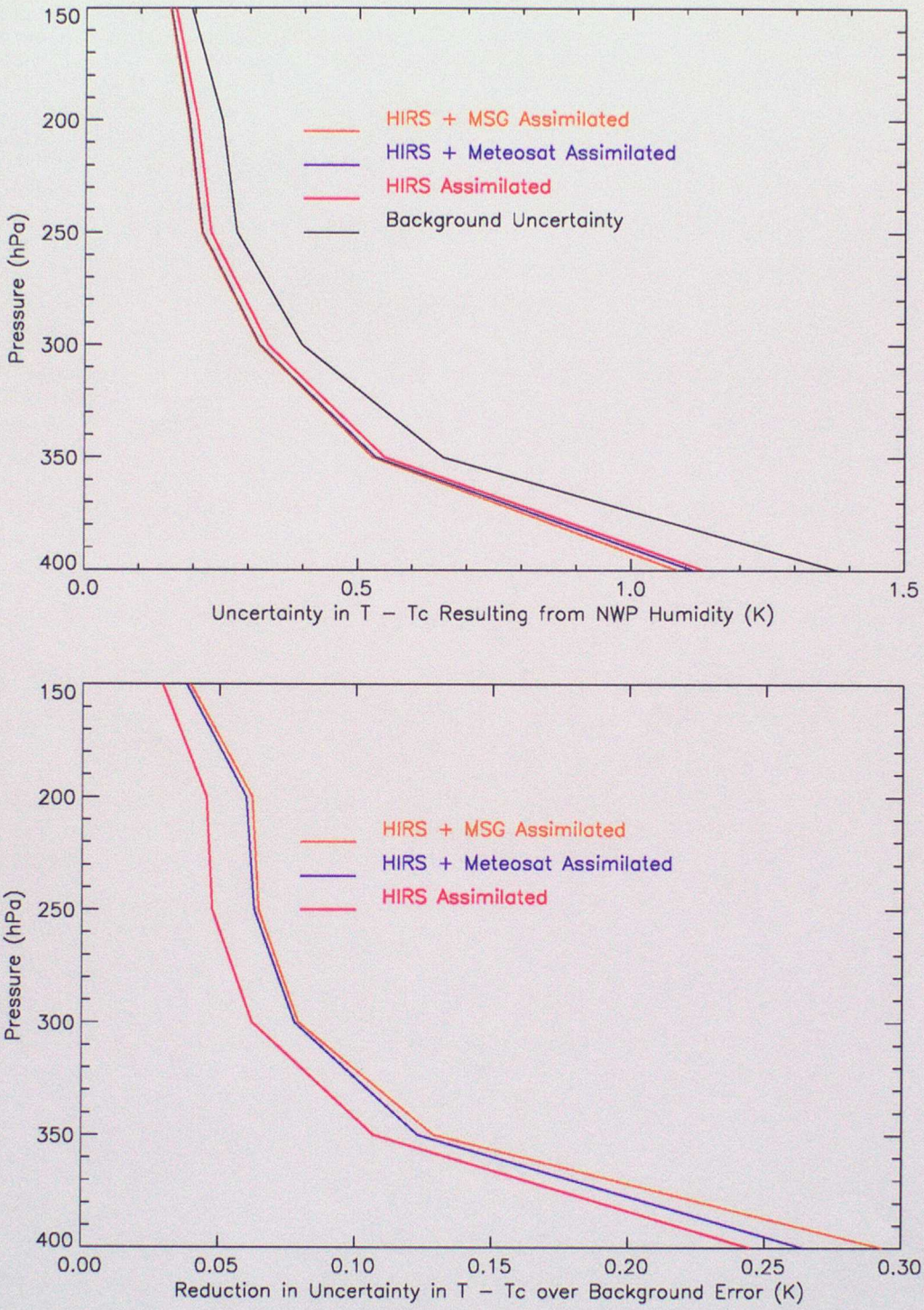

Figure 6: Upper graph shows the uncertainty in $T - T_c$ resulting from the expected error in model humidity fields, and the effect of the assimilation of satellite data on this quantity. T_c is the critical temperature for the formation of contrails. Lower graph shows the reduction in uncertainty relative to the model background error for different combinations of assimilated satellite data.

The upper graph in figure 6 shows the effect of the uncertainty resulting from NWP background error on the calculation of $T - T_c$. This analysis does not consider uncertainty in $T - T_c$ that results from errors in the temperature field. Also shown is uncertainty in $T - T_c$ after assimilation of the three combinations of satellite data. It can be seen that the assimilation of satellite data has the greatest effect on the uncertainty in $T - T_c$ at 400 hPa, where the assimilation of HIRS reduces the uncertainty from about 1.47 K to about 1.13 K. The assimilation of Meteosat or MSG only reduces the uncertainty further by a maximum of 0.05 K.

The lower graph in Figure 6 shows the reduction in uncertainty in $T - T_c$ relative to the background level. This demonstrates explicitly that the majority of the improvement is already gained through the assimilation of HIRS. Assimilation of Meteosat/MSG provides only a small further reduction in uncertainty.

These results confirm that the use of Meteosat/MSG data would do little to improve the quality of the contrail forecasts. The main reason for this is likely to be that the wavelengths of the Meteosat/MSG channels are similar to those of HIRS, resulting in weighting functions with similar pressure sensitivity.

6 Data assimilation issues for Meteosat

The results presented show that the ability of Meteosat data to correct an individual forecast is limited since HIRS data is already assimilated. The main advantage that Meteosat might offer is that the imagery is available hourly. In theory it might be possible to perform model analyses with a more up-to-date Meteosat image, making use of the good temporal resolution of the observations. In practice, this would be hard to achieve without incorporating the Meteosat image into the NWP model itself using 3D-var.

The Met Office plans to incorporate Meteosat (or MSG) WV channel information operationally when a 4D-var data assimilation system is in use rather than 3D-var. At this point it will become possible to take full advantage of the temporal resolution of this data source as the observation is compared with the model state at the time of the observations. This process will be done continuously allowing all of the hourly data to be assimilated.

The use of Meteosat data in adjusting relative humidity fields is also limited by the presence of clouds. The infrared wavelengths are strongly attenuated by clouds, whose presence causes a breakdown in the relationship between radiance and relative humidity. This means that in the use of infrared data there is a reliance on identifying pixels affected by cloud. Any errors in this process mean that the satellite data should be used with caution, particularly around the edges of clouds.

7 Conclusions

For borderline contrail formation situations, any improvement in the accuracy of the NWP humidity data would be reflected in the accuracy of the forecast outcomes. It was anticipated that up-to-date water vapour images from geostationary satellites could be used to nudge NWP humidity data towards greater accuracy. Results for Meteosat and Meteosat Second Generation show that assimilation of either of these data sources is unlikely to give any great improvement in forecast accuracy. This is because they are sensitive to water vapour over similar pressure ranges to HIRS channel 12, which is already assimilated operationally.

As stated in section 6, it is not yet possible to take full advantage of Meteosat data: the importance of geostationary weather satellites is in their temporal resolution. In the current 3D-var system, the major limitation of Meteosat is that it is an imager, not a sounder. In having only one water vapour channel, Meteosat is sensitive only to the layer-average relative humidity. There is no direct information on humidity at more specific levels in the atmosphere, limiting the use of these data in contrail formation prediction, which requires accurate humidity information on flight levels. This situation will improve only slightly with MSG's two water vapour channels.

Acknowledgements

I am very grateful to several Met Office colleagues in Satellite Applications–in particular Dave Jones, who suggested the method and provided enthusiastic help. I would also like to thank Caroline Poulsen, John Eyre and Roger Saunders for further assistance and comments.

References

Eyre, J. R. (1990). The information content of data from satellite sounding systems: a simulation study. *Q. J. R. Meteorol. Soc.*, 116:401–434.

Forrester, D. (2001). Private communication.

Ingleby, N. B. (2001). The statistical structure of forecast errors and its representation in the met office global 3-dimensional variational data assimilation scheme. *Q. J. R. Meteorol. Soc.*, 127:209–231.

Jackson, A., Newton, B., Hahn, D., and Bussey, A. (2001). Statistical contrail forecasting. *J. Appl. Meteorol.*, 40(2):269–279.

Poulsen, C. (2001). Private communication.

RTTOV-6 science and validation report (2000). http://www.metoffice.com/sec5/NWP/NWPSAF/rtm/svr81.pdf.

Saunders, R. W., Matricardi, M., and Brunel, P. (1999). An improved fast radiative transfer model for assimilation of satellite radiance observations. *Q. J. R. Meteorol. Soc.*, 125:1407–1425.

Schumann, U. (1996). On conditions for contrail formation from aircraft exhausts. *Meteorol. Z.*, 5(1):4–23.

Soden, B. J. and Bretherton, F. P. (1993). Upper tropospheric relative humidity from the GOES 6.7 μm channel: method and climatology for July 1987. *J. Geophys. Res.*, 98(D9):16669–16688.

A Acronyms

AIRS	Atmospheric Infrared Sounder
AMSU	Advanced Microwave Sounding Unit
ECMWF	European Centre for Medium-Range Weather Forecasts
EUMETSAT	European Organisation for the Exploitation of Meteorological Satellites
GOES	Geostationary Operational Environmental Satellite
HIRS	High Resolution Infrared Radiation Sounder
HSB	Humidity Sounder for Brazil
ICAO	International Civil Aviation Organisation
MSG	Meteosat Second Generation
NASA	National Aeronautics and Space Administration
NOAA	National Oceanic and Atmospheric Administration
NWP	Numerical Weather Prediction